Scalable Gaussian process regression enables accurate prediction of protein and small molecule properties with uncertainty quantitation

Jonathan Parkinson¹ and Wei Wang^{1,2}
¹Department of Chemistry and Biochemistry, ²Department of Cellular and Molecular Medicine, University of California, San Diego, La Jolla, CA 92093-0359

Correspondence to: Wei Wang, email address: wei-wang@ucsd.edu

ABSTRACT

Gaussian process (GP) is a Bayesian model which provides several advantages for regression tasks in machine learning such as reliable quantitation of uncertainty and improved interpretability. Their adoption has been precluded by their excessive computational cost and by the difficulty in adapting them for analyzing sequences (e.g. amino acid and nucleotide sequences) and graphs (e.g. ones representing small molecules). In this study, we develop efficient and scalable approaches for fitting GP models as well as fast convolution kernels which scale linearly with graph or sequence size. We implement these improvements by building an open-source Python library called xGPR. We compare the performance of xGPR with the reported performance of various deep learning models on 20 benchmarks, including small molecule, protein sequence and tabular data. We show that xGRP achieves highly competitive performance with much shorter training time. Furthermore, we also develop new kernels for sequence and graph data and show that xGPR generally outperforms convolutional neural networks on predicting key properties of proteins and small molecules. Importantly, xGPR provides uncertainty information not available from typical deep learning models. Additionally, xGPR provides a representation of the input data that can be used for clustering and data visualization. These results demonstrate that xGPR provides a powerful and generic tool that can be broadly useful in protein engineering and drug discovery.

INTRODUCTION

Identification of proteins and small molecules with desired properties is a task of crucial importance for the pharmaceutical and chemical industries¹. In recent years, machine learning assisted approaches have become more popular^{2–8}. Neural network/deep learning models are widely used owing to their flexibility, their ability to learn complex relationships from large datasets, and – owing to the development of libraries like Tensorflow and PyTorch – ease of implementation².

Despite deep learning's success, it suffers from several limitations. First, most deep learning architectures do not quantify their uncertainty on predictions, tend to be "over-confident" when extrapolating and are "black-box", so that it is very hard to determine why the model makes a particular prediction for a specific input⁹. A variety of approaches^{10–12} have been devised to estimate uncertainty on deep learning predictions but generally suffer from important limitations. Variational Bayesian neural networks for example provide approximate uncertainty but the quality of this approximation has been shown to be poor, resulting in unacceptable overconfidence in predictions for new data far from their training set¹³. Second, surprisingly, deep learning models have repeatedly been shown to lack robustness to so-called "adversarial attacks", small perturbations to their input. Adding subtle noise not perceptible to the human eye, for example, could reliably cause deep learning models to misclassify a photo of a cat as guacamole, or a lionfish as eggnog¹⁴. In biology, protein structure prediction models have been shown to exhibit the same vulnerability to adversarial attacks¹⁵. Finally, deep learning often entails enormous computational cost. Many state of the art models use tens or hundreds of

billions of learned parameters. Often a large fraction of their parameters can be removed without damaging performance, suggesting some more efficient approach is possible. Xu et al., for example, were able to prune *97%* of the parameters of the BERT model in natural language processing and still achieve equivalent performance¹⁶.

An alternative model architecture is Gaussian process (GP) regression¹⁷. A GP is a Bayesian model which defines a multivariate normal distribution over possible functions mapping the input x variable to an output y. In regions where there is little or no training data, the model expresses high uncertainty. In regions where there is substantial training data, the model predicts outcomes with more confidence. The type of functions in the distribution is determined by a kernel function that needs to be selected and its hyperparameters "tuned" (as with any other model) for a specific problem. The kernel function measures the similarity of any two x-inputs.

GP models have at least four compelling advantages. First, like deep learning, if equipped with an appropriate kernel, a GP is able to approximate any relationship. Second, GP can calculate the marginal likelihood – the probability of the data averaged over all possible function values – in closed form, because the integral needed to calculate this value can be solved analytically. Consequently, kernel hyperparameters can be tuned by maximizing marginal likelihood rather than the likelihood, reducing the risk of overfitting and thus making the model more robust. Third, the model's predictions are generated using the similarity of new data points to those in the training set, where similarity is quantified by the kernel function. Unlike a deep learning model, a GP is not a black box, because one can determine how the model measures similarity between datapoints and generates predictions. This enables practitioners to incorporate "prior knowledge" about the relationship between inputs and outputs into the model architecture.

Fourth, a GP reliably quantifies its uncertainty and assigns high uncertainty to datapoints very dissimilar from its training set. Uncertainty is important for protein engineering and drug design where experimentally evaluating model predictions is expensive. In these scenarios, one would rather use only model predictions that are more likely to be reliable. GP would detect "distribution shifts", where new data points are very different from the training set by assigning high uncertainty to its predictions, while a deep learning model may "fail silently", generating low-accuracy predictions without providing any obvious sign of failure^{9,18,19}.

Distribution shifts are a critical problem in many applications¹⁹. DeGrave et al., for example, found many deep learning models trained on data from specific hospitals to diagnose COVID-19 from chest radiographs failed catastrophically when labeling data from different hospitals²⁰. Images collected by different hospitals exhibited subtle differences, and this "distribution shift" confounded the models, but because the deep learning models do not quantify their uncertainty, they provided no indication that a shift had occurred. This problem is among the issues described by Roberts et al. who found that, of 62 models for detecting COVID-19, none were clinically useful.²¹

The main challenge for GP is computational expense. A straightforward implementation scales with dataset size as $O(N^3)^{17}$, while modern implementations scale as $O(N^2)^{22}$, where N is the number of datapoints. Frequently in the literature deep learning is chosen over a GP because of scaling. Li et al., for example, in describing their deep learning model for traffic prediction, briefly consider using a GP and argue that this is not possible because "GPs are hard to scale to a large dataset" A second major challenge is the lack of *efficient* kernels for sequence and graph data. Many kernels for graphs have been described²⁴, but typically exhibit quadratic or worse scaling in the size of the graph.

Several approaches for approximating a GP to reduce cost have been described. Some "sparse" methods use "inducing points", a set of points in the input space that is considerably smaller than the number of datapoints, to construct an approximate GP. Performance however depends on the number and location of the inducing points. Since these methods exhibit rapid increase in cost with an increasing number of inducing points, they are limited to a number of inducing points in the low thousands. This is often insufficient to accurately model a complex relationship.²⁵

One popular variant on this method is the stochastic variational Gaussian process (SVGP), which optimizes by maximizing a lower bound on the log marginal likelihood via stochastic gradients²⁶. Both the hyperparameters of the kernel and the locations of the inducing points are optimized simultaneously. This creates a complicated optimization problem; it has been shown that the optimizer may become trapped in local minima during training of this type of model, causing subpar performance²⁷. We show in the Supplementary Info (Section S2, Table S2) that in practice, the SVGP when equipped with the same kernel generally achieves both worse performance and significantly longer training time as compared with other approximations.

Another prominent approach approximates the kernel function using Monte Carlo sampling, the random Fourier feature (RFF) approach of Rahimi and Recht²⁸. Briefly, RFF methods approximate the kernel function via a random map corresponding to the kernel of interest, so that each input datapoint is converted into a "random feature" representation; one is then able to approximate the Gaussian process using linear regression in the random feature space. As the size of the random map increases, so too does the accuracy of the approximation, but with diminishing returns. The size of the random map required to achieve a good approximation can be large; while this approach achieves linear scaling in the number of datapoints, it nonetheless remains expensive for many tasks.

In this paper, we develop strategies for reducing the cost of fitting a GP and efficient kernels for graphs and sequences. We implement all these improvements in an open-source Python library, xGPR, and evaluate it on 20 benchmarks from the literature, including protein sequence, small molecule and tabular data.

RESULTS

To achieve fast and accurate modeling with approximate GPs, we have developed

- 1) a new preconditioner that reduces the cost of fitting a GP with a given set of kernel hyperparameters ("fitting") by orders of magnitude.
- 2) novel strategies for tuning the hyperparameters ("tuning") that reduce the cost of tuning by up to 10 fold.
- 3) a novel fast approach for random feature-based convolution.

Furthermore, to analyze large sequence and graph data of proteins and small molecules, we have introduced a novel convolution kernel whose structure is analogous to a three-layer convolutional neural network, a novel, flexible approach for modeling graphs with a GP and a fast approximation to a popular kernel for small molecules.

We implement all of our improvements in an open-source library, xGPR, and evaluate its performance on 20 benchmarks of diverse data. We show that xGPR provides similar or better accuracy to state of the art deep learning models while providing additional uncertainty on the predictions. We also incorporate an easy-to-use tool for extracting a representation of the input

from a trained model that can be used for data visualization and clustering. All of the datasets used in this paper are publicly available and are described in more detail in the Supplementary Info section S1, Table S1. Some of the experiments performed in this paper are also further illustrated as demos in the xGPR documentation, available online at https://xgpr.readthedocs.io/en/latest/.

Achieving fast fitting

In a typical Gaussian process model (see ref ¹⁷ for details), given a training set X with associated y-values, we make predictions for the y-value f_* associated with a new datapoint x_* :

$$p(f_* \mid X, y, x_*) = N(u_*, \sigma_*)$$

where $N(u_*, \sigma_*)$ is a Gaussian distribution with mean and variance of

$$u_* = k_*^T (\lambda^2 I + K)^{-1} y$$
 and $\sigma_* = k_{**} - k_*^T (\lambda^2 I + K)^{-1} k_*$

Here k_* is a vector of length N for N training datapoints formed by evaluating the kernel function $k(x_*, x_i)$ for each x_i in the training set, and K is an N x N matrix where element ij is formed by evaluating the kernel function for $k(x_i, x_j)$ points in the training set. λ^2 is a kernel hyperparameter which denotes the level of expected noise in the data. k_* is the kernel function evaluated on the new datapoint against all training datapoints, and k_{**} is the kernel function evaluated on the new datapoint against itself. When fitting, we do not have to "learn" any parameters, but we do have to invert an N x N matrix, which is extremely expensive if N is large.

Implementation of fast approximation of kernel function using random Fourier features To avoid this cost, we approximate the kernel function using random Fourier features²⁸. This approximation specifies a random map for a given kernel such that $k(x_1, x_2) \approx z(x_1)^T z(x_2)$ (for details, see Online Methods and Supplementary Info S3). The mean and variance are now predicted for new datapoints using:

$$\mu_* = z_*^T [Z^T Z + \lambda^2 I]^{-1} Z^T y = z_*^T w, \qquad \sigma_* = \lambda^2 z_*^T [Z^T Z + \lambda^2 I]^{-1} z_* = \lambda^2 z_*^T V z_*$$
 (1)

Where Z is the transformed input matrix, such that row i is $z(x_i)$ and z_* is $z(x_*)$ where x_* is a new datapoint, λ is a kernel hyperparameter. For common stationary kernels, the error of the approximation decreases exponentially with an increasing number of random features²⁸; for example, going from 1,000 to 2,000 random features improves model performance significantly and adding more random features gains less and less improvement.

For a small number of random features, the equations in (1) can be solved by matrix decomposition¹⁷. This simple approach however has O(NDM) time complexity to generate the random features and $O(NM^2)$ complexity to fit, where N is the number of datapoints, D is the dimensionality of the input, and M is the number of random features.

To reduce the computational cost, we first incorporate the structured orthogonal random features (SORF) procedure²⁹. Briefly (for details, see the Online Methods and Supplementary Info Section S4), with the RBF kernel as an example, the following transformation is applied to each input vector:

$$SHD_1HD_2HD_3$$
 (2)

Where S is a diagonal matrix with elements drawn from a χ -distribution with d degrees of freedom, H is the normalized Hadamard matrix, and D_1 , D_2 , D_3 are diagonal matrices with elements drawn from the Rademacher distribution. We next replace the Hadamard matrix with a fast Hadamard transform³⁰ to reduce the cost of generating the random features to O(NMlogM). The resulting model is extremely lightweight, since we only need to store four diagonal matrices. Generating predictions is fast, since we need only perform a series of fast transforms & diagonal matrix multiplications, then take a dot product – no matrix multiplication is required.

Since there are no efficient implementations of the Hadamard transform in major Python scientific computing libraries, we write an implementation for CPU and GPU. Compared to the matrix multiplication in the Numpy and Cupy libraries (Supplementary Info Section S5), our implementation is faster for modest numbers of random features, and the performance advantage increases with larger numbers of random features as expected (Table S3 and S4).

Separate numbers of random features for predicting mean and variance

xGPR allows specifying separate numbers of random features for predicting mean and variance, which avoids incurring a large expense calculating σ_* when only an approximate result is sufficient. As we will illustrate below under "The Benefits of Uncertainty", a large increase in uncertainty indicates a "distribution shift" or an unreliable prediction even if the variance is only approximately calculated.

In most applications, the accuracy of mean μ_* (the predicted value) is more important than the accuracy of variance σ_* . For predicting μ_* as accurately as possible, we may need to scale to a large number of random features. Consequently, we adopt the method of conjugate gradients³¹, which achieves subquadratic scaling in the number of random features and iteratively solves

$$b = Aw$$
 for w. Note that $[Z^TZ + \lambda^2 I]w = (\sum_{i=1}^{N} z_i^T z_i + \lambda^2 I)w$ for N row vectors in Z; in other

words, the matrix vector product can be formed as a sum of outer products over individual rows. We therefore loop over the dataset in "chunks", loading a chunk of data into memory at a time. For each chunk, we generate the random features using the Hadamard transform-based procedure and perform a matrix-vector multiplication then add this to the result. We can control our memory footprint by choosing the chunk size, i.e. how many datapoints to load at a time, and thus in theory can analyze any size of data.

Our implementation also allows easy scaling to multiple GPUs or CPUs. On each iteration of conjugate gradients, each worker can be assigned its own copy of the kernel, its own copy of w, and its own subset of the data to process. At the end of the iteration, the results from all the workers are summed and used to update w for the next iteration.

A new preconditioner for fast approximation of matrix inverse

To ensure a fast convergence, xGPR uses a new preconditioner that approximates the inverse of the matrix $[Z^TZ + \lambda^2I]^{32}$ in equation (1). The better it approximates the inverse of this matrix, the fewer iterations are required to converge. Kernel matrices for Gaussian processes can be approximated using the Nystrom method (for details, see the Online Methods and Supplementary Info Section S6). We instead use it as a preconditioner for a random feature approximation of a Gaussian process.

We implement the randomized Nystrom approximation³³ because our initial experiments showed it provided better performance than the "classic" Nystrom approximation. We also incorporate a novel modification to the randomized Nystrom approximation wherein we replace a matrix multiplication with a fast Hadamard transform-based procedure, which greatly reduces the time needed to construct the preconditioner, and an algorithm using two passes over the dataset rather than one, which results in a better preconditioner. See the Online Methods and Supplementary Info Section S6 for the details of our implementation and an evaluation of our improvements. Importantly, in our implementation the preconditioner can be constructed by loading only one chunk of the data into memory at a time, enabling us to minimize our memory footprint. This approach provides a rank-L approximation to A; the larger L, the better the approximation, and the greater the improvement in rate of convergence is likely to be. Under Online Methods, we outline a simple strategy for choosing L.

Benchmarking the approach

In Figure 1a, we compare our preconditioned conjugate gradient (PCG) approach using different rank numbers with L-BFGS across 7 datasets; L-BFGS (limited memory BFGS) is a popular algorithm for minimizing the loss function with an iteratively constructed approximation to the Hessian³⁴. The PCG strategy reduces the number of iterations required for convergence and hence the cost of fitting by as much as *two orders of magnitude* compared with L-BFGS, enabling us to achieve a tight fit in as few as 10-20 epochs for some datasets.

In Figure 1b we further compare our PCG approach with stochastic variance reduced gradient descent (SVRG)³⁵ using the new preconditioner for acceleration (PSVRG), implemented as an option in xGPR. SVRG reduces the variance of gradient descent using a "snapshot" gradient acquired every other epoch, and we can use the same preconditioner to accelerate it as well. We also compare with AMSGrad, an improved variant of the Adam algorithm which is popular for training neural networks.

As illustrated in Figure 1b, our preconditioner also greatly accelerates SVRG, although SVRG requires extensive step size tuning unlike PCG and may still underperform. AMSGrad performs poorly and is not competitive with either approach. This analysis shows that PCG is the clear winner. As we will demonstrate below under "Evaluating xGPR performance: Tabular data", our PCG approach enables us to fit datasets of half a million datapoints with 32,768 random features in < two minutes on a single GPU, including preconditioner construction, and as discussed above, xGPR can scale to much larger datasets.

Efficient hyperparameter tuning

It is possible to tune hyperparameters of a Gaussian process in the same way that hyperparameters for neural network models are often tuned – by fitting the model for different hyperparameter combinations, evaluating performance on a validation set for each combination, and choosing new combinations using an optimization algorithm. This strategy has been very widely used for tuning hyperparameters for other machine learning models^{37–40} and is supported in xGPR but is not our preferred approach. One of the advantages of a Gaussian process is the

ability to tune hyperparameters by minimizing the negative marginal log likelihood; this means to maximize the probability of the data averaged over all possible function values for a given set of hyperparameters. This approach has a greatly reduced risk of overfitting, especially for small datasets. We now outline two novel methods that reduce the cost of hyperparameter tuning with marginal likelihood.

In the random feature scheme the negative marginal log likelihood is as follows:

$$-\log p(y \mid X) = \frac{-1}{2\lambda^2} y^T Z (Z^T Z + \lambda^2 I)^{-1} Z^T y + \frac{1}{2\lambda^2} y^T y + (n - m) \log(\lambda) + \frac{1}{2} \log|Z^T Z + \lambda^2 I| + \frac{n}{2} \log(2\pi)$$
(5)

In our first approach, we note that Z^TZ is Hermitian so that as long as it is full-rank, we can generate an eigendecomposition $P\Lambda P^T$ such that P is orthonormal, i.e. $PP^T = I$. We rearrange the above expression:

$$-\log p(y \mid X) = \frac{-1}{2\lambda^2} y^T Z P \left(\Lambda + \lambda^2 I\right)^{-1} P^T Z^T y + \frac{1}{2\lambda^2} y^T y + (n-m) \log(\lambda) + \frac{1}{2} \log|\Lambda + \lambda^2 I| + \frac{n}{2} \log(2\pi)$$
(6)

Many popular kernels (indeed, all the convolution kernels we introduce in this paper, and all of those currently implemented in xGPR) have three hyperparameters – one that is specific to the kernel, then λ^2 and the "amplitude" of the kernel – what we will call β . Each row of Z is ordinarily multiplied by β during random feature generation. In xGPR, we can compute the eigendecomposition of Z^TZ using selected values for the hyperparameters specific to that kernel, but without multiplying by β before performing the eigendecomposition. We store y^TZP , Λ and y^Ty to cheaply compute the negative marginal log likelihood for any value of β and λ . This allows to find optimal values of β and λ for a given set of kernel-specific hyperparameters without conducting any further matrix decompositions or passes over the data. This is important, because each matrix decomposition and each pass over the data is expensive.

We use this modification to run Bayesian optimization³⁶, which is highly efficient for 1d spaces, over the kernel-specific hyperparameter; for each suggested set of kernel-specific hyperparameters, we conduct one pass over the data and find optimal values of β and λ without any further passes required. We describe this algorithm in more detail in the Supplementary Info Section S7. The strategy we propose here is novel to our knowledge.

To assess the performance of this strategy, in Table 1 we compare the number of effective iterations (passes over the dataset) required to find the global minimum for the RBF kernel across 5 tasks using either the approach described above or L-BFGS with 5 restarts. We see that the new strategy is able to achieve the same result as the classic approach to tuning hyperparameters for Gaussian processes, L-BFGS with multiple restarts (also implemented in xGPR). L-BFGS, however, requires 140 - 200 passes over the data, while our Bayesian approach requires 16 - 18 – an order of magnitude reduction in computational expense.

While this strategy is efficient, since it requires matrix decompositions, it exhibits poor scaling to large numbers of random features and to large datasets, and it is generally useful for up to

4,000 - 5,000 random features at most. To overcome this drawback, we implement a second novel strategy in xGPR.

Consider again equation (5). Disregarding irrelevant constants, there are two key terms:

$$\frac{-1}{2\lambda^{2}}y^{T}Z(Z^{T}Z + \lambda^{2}I)^{-1}Z^{T}y$$
 (7)

$$(n-m)log(\lambda) + \frac{1}{2}log|Z^TZ + \lambda^2I|$$
 (8)

The first term involves fitting the model by finding $(Z^TZ + \lambda^2 I)^{-1}Z^Ty$, which can be done efficiently using our preconditioned conjugate gradients strategy without ever loading more than one chunk of data to memory at a time. To deal with the second term, rather than using matrix decompositions we can estimate the log determinant using stochastic Lanzcos quadrature³⁷ The tridiagonal matrix required for SLQ can be populated using information generated by the preconditioned conjugate gradients (PCG) algorithm at negligible additional cost (see Saad 2003 for details)³². SLQ has been used in concert with PCG to estimate log determinants for exact (unapproximated) Gaussian processes by Gardner et al.²², but has never been used in combination with the random features approximation as we suggest here to our knowledge.

In xGPR, we have therefore implemented batched preconditioned conjugate gradients to calculate both (7) and (8), thereby achieving linear scaling with dataset size and subquadratic scaling with number of random features for marginal likelihood calculations. To evaluate the accuracy of this procedure, we randomly select 8 hyperparameter combinations each for 7 different datasets ranging in size from a few hundred datapoints to half a million. For each, we calculate the negative marginal log likelihood with 4,096 random features either using equation 10 or using the SLQ-based approach. The results appear in the Supplementary Info section S8. In every case, the error in the approximation is < 0.02%.

As a general strategy, it is possible to use the less scalable matrix decomposition-based approach described earlier with a small number of random features to find a starting point, then to further optimize this starting point using Bayesian optimization to choose successive hyperparameter combinations and calculate the negative marginal log likelihood for each using the SLQ-based method with a larger number of random features (to provide improved accuracy in estimation). This general strategy is implemented in xGPR. An overall suggested workflow for tuning and fitting in xGPR is illustrated in Figure 2a, and we use this workflow in all of the experiments below under the "Evaluating xGPR performance" subsections.

Surprisingly, we are often able to outperform deep learning models using merely the starting point from the first phase alone without any need for further optimization. A possible explanation lies in the relationship between performance and number of random features. In xGPR, hyperparameter tuning is conducted separately from and prior to fitting. Importantly, we do not need to use the same number of random features for both fitting and tuning. Figure 1c shows the mean absolute error (MAE) of models tuned on three datasets from the UCI machine learning repository as a function of the number of random features used either for tuning using marginal likelihood maximization or for fitting. Note that we can improve performance by either increasing the number of random features for tuning *or* for fitting. Interestingly, performance-gains associated with more random features for tuning plateaus much more rapidly than the performance-gains associated with more features for fitting, at least when using

marginal likelihood maximization. This may explain why the starting point from the first phase of tuning is often sufficient to achieve good performance.

New kernels for protein sequence and small molecule data

Efficient implementation of a convolution kernel for sequence data

We develop a new convolution kernel for sequence data and time series called FHTConv-1d, which is an efficient implementation of a random feature-based 1d convolution kernel described by Morrow et al. (referred to as Conv-1d henceforth)³⁸. It approximates the following kernel:

$$\sum_{i}^{d-n}\sum_{j}^{d-n}e^{-\gamma f(x_{i:i+n'},y_{j:j+n})}$$

Where f is the square of the L2 distance, x and y are input sequences, d is sequence length and n is convolution width. This is just the sum of an RBF kernel evaluated pairwise across subsequences in the two inputs; the two inputs can trivially be zero-padded to be the same length. We note that it is possible to use another kernel for the pairwise comparisons, e.g. Matern or arc-cosine, although we only implement and evaluate the performance of the

RBF-based Conv-1d at this time. Conv-1d approximates the above kernel as $(\sum_{i}^{d-n} z_i)^T (\sum_{j}^{d-n} z_j)$, and thereby achieves linear scaling in both datapoints and sequence length.

While powerful, this kernel requires either thousands of convolutions per iteration or a large disk space footprint. Moreover, if the number of features associated with each sequence element is large, the Conv-1d kernel will suffer from increased computational cost.

Just as we did for the RBF kernel, we replace the matrix of convolution filters with the SORF operation in FHTConv-1d:

$$SHD_1HD_2HD_3$$

Where S, D1, D2, D3 are diagonal matrices and H corresponds to the normalized fast Hadamard transform. In deep learning libraries convolution is often implemented using matrix multiplication. Let the number of features d associated with each subsequence be a power of 2, which can be achieved by zero padding. For simplicity, let the number of random features desired, m, be the same as d. If m is less than d, we can generate d random features and discard the excess; otherwise, generate d random features x times where x is the result of ceiling division of m by d. In this case, the cost of the random feature convolution operation scales as $O(NKm^2)$ where K is the number of subsequences in each sequence. FHTConv-1d by contrast scales as $O(NKm \log m)$. Obviously, FHTConv-1d is faster if the convolution width or the number of features per sequence element is large, and dramatically reduces memory footprint. In the section "Evaluating xGPR performance: Small molecules" section below, we describe an experiment in which we fit a convolution kernel with ~65,000 random features to graph data where each vertex has ~18,000 features. Conv-1d would require storing a matrix containing about 1.2 billion floats, whereas FHTConv-1d has a memory footprint that is roughly 8.000-fold smaller.

In theory, FHTConv-1d should offer prediction accuracy similar to or better than Conv-1d, since the SORF approach is a lower-variance approximation of an RBF kernel than standard random

features (see Choromanski et al.³⁹), and the convolution kernel is a sum of RBFs. Figure 1d compares the performance of FHTConv-1d with Conv-1d across a series of protein property prediction problems discussed under the benchmarks section; prediction accuracy is very similar. Both FHTConv-1d and Conv-1d are implemented in xGPR so the user can select the Conv-1d kernel if the number of features associated with a sequence element is small, or FHTConv-1d if it is large.

A new kernel for sequence data

We have also developed a novel kernel called FastConv-1d in xGPR. We make use of the following simple lemma (see the Supplementary Info Section S9 for a proof):

<u>Lemma 1.1.</u> Let $K: \mathbb{R}^D x \mathbb{R}^D \to \mathbb{R}$ be a positive definite kernel on \mathbb{R}^D , and let $f: X \to \mathbb{R}^D$ be any mapping from X to \mathbb{R}^D , where X is some non-empty set. Then K(f(u), f(w)) is a positive definite kernel for all $u, w \in X$.

Consider a three-layer neural network with random weights where the first layer is a convolutional layer with ReLU activation followed by global max pooling and the second layer is fully-connected with trigonometric activation functions. This is analogous to an RBF kernel whose input is a random feature convolution with ReLU activation and global max pooling (Supplementary Figure S4). This combination kernel is positive definite following lemma 1.1. This kernel has the property that the convolutions can all be performed exactly *once* before training and the results saved on disk; these results are then used to fit the kernel used in the GP such as the RBF or Matern kernel.

Benchmarking the kernels on sequence data

Figure 1d compares the performance of the Conv-1d kernel with FastConv-1d and FHTConv-1d on a set of protein sequence tasks. FastConv-1d achieves similar performance on these tasks but is substantially faster for hyperparameter tuning.

FastConv-1d and Conv-1d / FHTConv-1d quantify distances between sequences in fundamentally different ways. FastConv-1d quantifies the distance between sequence profiles generated by convolution with random weights. Conv-1d / FHTConv-1d by contrast approximates an averaged RBF kernel applied pairwise across all length *d* subsequences in the two inputs. The FHTConv-1d is thus more applicable to problems where the similarity between subsequences, averaged over *all* subsequences in both sequences, is an appropriate way to quantify similarity. Both kernels are provided as options in xGPR.

Efficient, numbering-invariant kernel for small molecules and other graphs

We develop and implement new kernels for small molecule and graph data in xGPR. Each atom of a molecule or a node in a graph has associated features such as atom type and descriptors of the atom's neighbors or chemical environment.

We introduce a novel approach: we use the features associated with each atom (or other local environment) to a convolution kernel of width 1, using the FHTConv-1d kernel from above. This is an efficient approximation to averaging across an RBF kernel evaluated pairwise across all pairs of environments in the two graphs, which is $O(N^2)$ and $O(D^2)$. Our approach reduces the complexity to O(N) in dataset size and O(D) in graph size – an *enormous* savings in cost for large datasets. This kernel is numbering invariant; because the random features for each node are summed it does not matter how the nodes of the graph are numbered. We examine the performance of this approach under the benchmarks section below.

As for sequences, we can also perform a pairwise evaluation across all environments in the two graphs using a different kernel, and build a similar linear-scaling approximation using random features. Notably, polynomial kernels have occasionally been used in this fashion for graphs. The SOAP kernel of Bartok et al.⁴⁰ for example is essentially a polynomial kernel evaluated pairwise across each pair of atoms in two molecules before summing the results. In the Supplementary Info section S10, we describe a novel approach to approximate a polynomial kernel evaluated pairwise on vertices of two graphs that reduces scaling with graph size from $O(D^2)$ to O(D), a huge reduction in cost. This kernel is more specialized in analyzing certain problems for small molecule or graph data. It is implemented in xGPR as the GraphPoly kernel.

Evaluating xGPR performance: Protein sequences

Determining which kinds of problems are best suited for GPs as opposed to deep learning or gradient boosted trees is a very broad question beyond the scope of this paper. Our goal here is merely to demonstrate that the xGPR library can be useful for a variety of problems related to proteins, small molecules and tabular data. We use only regression data since xGPR is not currently configured to perform classification (for reasons we discuss in the Discussion). The code is available at https://github.com/Wang-lab-UCSD/benchmarking_xGPR.

We first consider 11 protein engineering benchmarks from Rao et al. and Dallago et al. 41,42 (the TAPE benchmarks and FLIP benchmarks respectively). Results are shown in Table 2. In these comparisons, we *only* use one-hot encoded sequence data as inputs and *only* compare against deep learning models that also use one-hot encoded inputs. This is to ensure that we are assessing models not representations. We tune the hyperparameters in triplicate and fit in triplicate using different random seeds; the resulting error bar measures variability across different random seeds. The results illustrate that variability across random seeds is negligible. We also fit in triplicate using either 8,192 random features or 16,384 random features, to examine the impact of this selection. For more details, see the Online Methods section.

In 7 out of 11 cases, including the two largest datasets, GP models outperform deep learning models trained on the same inputs (we use the model performance reported by Dallago et al⁴² and Rao et al⁴¹ for the deep learning models). In all of these cases, the GP models outperform the deep learning model using 8,192 random features, and switching to 16,384 features increases the margin by which the GP outperforms the deep learning model. In another two cases, there is a tie. The FastConv-1d and FHTConv1d kernels train on all datasets in 8 minutes or less, *including* hyperparameter tuning, on a single Nvidia GPU. The results suggest that xGPR can frequently outperform standard deep learning models for sequences at modest computational cost, even when the features are uninformative.

Dallago et al. and Rao et al. also report performance "pretrained" deep learning models. A well-chosen pretrained model or learned representation can improve the performance of both a deep learning model and a GP on a given task. There are many issues involved in choosing a learned representation that are beyond the scope of this study (see Detlefsen et al.⁴³). For this reason, we defer consideration of other representations to future work.

We note in passing however that GP models trained on one-hot encoded data match or outperform state of the art pretrained models on 6 of these benchmarks, including the largest one (see Supplementary Info Tables S5, S6 and S7). This is surprising since the pretrained model has access to a substantial amount of additional information from pretraining on a large corpus. On the AAV dataset, designed-mutant split, for example, the FastConv-1d kernel

achieves a Spearman's *r* of about 0.78, whereas the best result for a pretrained deep learning model is 0.71. The GP model trained in under 8 minutes including hyperparameter tuning, while Dallago et al. reported that the pretrained deep learning model required 50 GPU-days of training time. Since the pretrained deep learning model unlike xGPR is not uncertainty-aware, it is unclear what benefit if any the pretrained model offers for this task.

Evaluating xGPR performance: Tabular data

Next, we evaluate xGPR on tabular data in Table 3. Shwartz-Ziv et al. have demonstrated that gradient boosted trees models frequently outperform deep learning models on this type of data. We use three regression tasks for tabular data benchmarks from Shwartz-Ziv et al.⁴⁴ and Schafl et al.⁴⁵. We do not evaluate classification tasks since xGPR only performs regression for now. Results appear in Table 3 below, as compared with state of the art deep learning models and XGBoost. The deep learning models are DNF-NET⁴⁶, TabNet⁴⁷, a 1d-CNN⁴⁴ and Hopular⁴⁵. For further details on the evaluation procedure, see the Online Methods section.

We note that for the YearPrediction dataset, the UCI machine learning repository indicates that a certain subset of the data should be used for testing, and not all benchmarks in the literature appear to have followed these instructions. Even with this caveat, however, xGPR outperforms achieves highly competitive results.

Evaluating xGPR performance: Small molecules

We next consider the prediction of energetic and thermodynamic properties of small molecules. We focus on these for two reasons. First, the internal energy is a key quantity required for MD simulations. Second, these can in principle be decomposed into a sum of per-atom contributions. This suggests our graph kernels are likely to be a good fit for this problem.

We benchmark on the QM9 dataset of Ramakrishnan et al.⁴⁸, which contains 134,000 small molecules whose geometry has been optimized using density functional theory (DFT). This dataset has been widely used to benchmark models for prediction of energetics and other properties as well. We use the smooth overlap of atomic positions (SOAP) features as implemented in the dscribe⁴⁹ library in Python. These features use a basis set expansion to represent the environment of each atom and share many similarities with the featurizations used as input by many of the deep learning models. For more details, refer to Online Methods.

We tuned hyperparameters for both the GraphConv-1d kernel and the GraphPoly kernel with a polynomial degree of 2 using marginal likelihood on the training set. The GraphConv-1d kernel achieved a slightly better log marginal likelihood (improvement of about 0.7%) and we therefore used GraphConv-1d, although the similarity of the marginal likelihood score suggests that GraphPoly would likely achieve very similar performance. The final results on the test set appear in Table 4, using either 16,384, 32,768 or 65,536 random features for fitting. We see that xGPR outperforms or matches most state of the art deep learning models on 4 of the 6 properties and matches or outperforms all deep learning models on two properties. It is able to achieve highly competitive performance with just 16,384 random features although as expected performance with larger numbers of random features continues to improve.

For internal energy, enthalpy and Gibbs free energy, xGPR can achieve an MAE < 0.2 kcal/mol. Note that 1 kcal/mol is typically considered to be "chemical accuracy", i.e. the accuracy required to make correct predictions for the behavior of chemical systems, so that both xGPR and several of the other models are well above the level of accuracy that is actually needed. Indeed, the density functional theory (DFT) calculations whose outcome we are trying to predict are

often only accurate to 2-3 kcal/mol. Consequently, a difference of 0.01 - 0.05 kcal/mol between models for predicting DFT-calculated energies is likely equivalent for practical purposes.

Even using the SOAP scheme, which generates about 18,000 features per atom, xGPR is faster than many comparable neural network models. The HMGNN model, for example, takes 3-4 days to train, whereas tuning hyperparameters for xGPR using the "fine-tuning" procedure with approximate marginal log likelihood takes < 4 hours on an A6000 GPU, and fitting using the largest number of random features used in this experiment took slightly over an hour. Moreover, developing a deep learning models requires complicated and lengthy experiments to choose the number of layers, the architecture, the learning rate schedule and so forth, whereas for xGPR the choices involved are fewer and more straightforward. As discussed in Online Methods, recent literature suggests we may be able to use a much more compact representation than the SOAP features to achieve similar results^{55,56}, and this would result in much faster training. We defer exploration of this possibility to future work.

Finally, it is interesting to note that using one-hot encoded atom types as inputs, without any more sophisticated feature representation, the GraphConv-1d kernel is able to achieve close to chemical accuracy (mean absolute error of < 1.1 kcal/mol) for internal energy prediction on the QM9 dataset. This experiment can be reproduced using the small molecule tutorial in the xGPR documentation, available online at https://xgpr.readthedocs.io/en/latest/.

The benefits of uncertainty

In addition to competitive accuracy and speed, Gaussian processes offer reliable uncertainty quantitation. We now briefly illustrate some of the insights this can provide. Consider Figure 2b, which plots binned uncertainty vs mean absolute error across three benchmark datasets. The figure also shows the distribution of uncertainty across training and test set predictions.

For the UCI protein dataset, both training and test predictions have similar uncertainty. For the fluorescence and AAV datasets on the left, by contrast, many of the test set datapoints have much higher uncertainty than the training set. This indicates many of these datapoints lie in a region of the space outside the training set. If we were to see this when processing new data, we could conclude a "distribution shift" had occurred – the model is telling us the new data is different from the training set.

As illustrated in the top panels, the predictions about which the model is least confident are also those which are least accurate; high uncertainty predictions are usually incorrect predictions. This enables us to quickly assess the reliability of predictions for new data. Again, we note that none of the deep learning model comparators in this study provide this kind of well-calibrated uncertainty information.

Visualizing and clustering data

For each input datapoint, xGPR generates a random features representation. Much like the embeddings from neural networks, this representation can be used for PCA and clustering. The PCA plots that are generated approximates a kernel PCA on the original data ⁵⁰, while clustering with k-means, for example, approximates kernel-k-means clustering of the input ⁵¹. In xGPR, we implement a tool for recovering the top *n* principal components in random features space for clustering or kernel PCA plots generation. This can help extract insights about the distribution of the data and how the model makes predictions.

It is beyond the scope of this paper to explore all possible applications; we restrict ourselves to an illustrative example, described under Supplementary Section S13 and in Supplementary Figures S5 and S6. Using the one-hot encoded QM9 small molecule dataset discussed under "Evaluating xGPR performance: Small molecules", we fit an xGPR model with a GraphConv-1d kernel, then perform kernel PCA and k-means clustering on the resulting representations. We see the first principal component correlates with energy at 298K. The resulting clusters correspond to overlapping but distinct ranges of energy values, and also correspond to crude measures of molecular polarity (e.g. TPSA). Thus we see the representation generated for each input datapoint by xGPR can also be used for clustering and visualization, and these operations can provide insights about the kernel and the distribution of the data.

DISCUSSION

Gaussian processes represent a principled Bayesian approach to machine learning that provides straightforward quantitation of uncertainty. Their chief disadvantages are their unacceptable scaling and the lack of efficient kernels for sequences and graphs. We develop an open-source library to overcome these problems. We achieve 1) linear time complexity in the number of datapoints, 2) sub-quadratic scaling in the number of random features, 3) efficient hyperparameter tuning, and 4) the ability to scale to datasets of any size. Additionally, we introduce fast new kernel approximations for sequence and graph data. Finally, we demonstrate that our library provides highly competitive performance.

We have discussed only regression in this paper. Classification for GP typically entails learning a "latent value" associated with each datapoint and having one Gaussian process per class label¹⁷. This results in a dramatic increase in computational cost. While alternatives have been suggested (e.g. Milios et al.)⁵², we are not aware of any at this time that would enable us to achieve the speed and performance we have achieved for regression. Consequently the xGPR package does not include tools for classification at this time.

A broad remaining question is what types of problems are best suited for GPs as opposed to deep learning, gradient boosted trees or other models. We here suggest as a hypothesis a simplified way of thinking about these models that may sometimes be useful.

A deep learning model for regression maps from inputs to some \mathbb{R}^D space, then takes the dot product with a set of learned weights. It can therefore be thought of as linear regression with automated feature engineering. A GP, by contrast, maps the input into some space such that a dot product in the space corresponds to a kernel that measures similarity. This simplified comparison suggests deep learning is most useful when we do not know how to design good features, in which case it provides efficient "black box" feature engineering. A GP, by contrast, is most useful if we have some existing measure of similarity appropriate for a given problem.

This hypothesis suggests that GPs can be useful for many problems involving proteins and small molecules, since there are existing useful measures of similarity that have been defined in bioinformatics and cheminformatics. For example, both our GP and the previous work of Willatt et al.⁵³ demonstrate that GPs perform quite well for predicting energetic and thermodynamic properties of small molecules, using an existing measure of similarity defined via SOAP features, and we here show that GPs can in many cases outperform comparable neural networks trained on the same features for protein engineering tasks. It may be interesting to try to extend these results to other protein and small molecule property prediction problems. We regard this, together with extension to classification, further efficiency improvements, and development of additional useful kernels, as interesting areas for further work.

ONLINE METHODS

We here provide additional key details for each section from Results. Each topic is additionally covered in the Supplementary Info in more depth as indicated and in the xGPR documentation at https://xgpr.readthedocs.io/en/latest/.

Achieving fast fitting

The random feature approximation specifies a random map for a given kernel such that $k(x_1, x_2) \approx z(x_1)^T z(x_2)$. Briefly (for details, see the Supplementary Info Section S3), consider an N x D input training matrix X where each row i is a D-dimensional vector corresponding to datapoint i and M is the number of random features we generate which is often << the number of datapoints. In this approach, a D x M matrix Q is populated with random features drawn from a kernel-specific distribution. Consider the popular RBF kernel:

$$k(x_{1,}^{T}x_{2}) = e^{-\gamma(x_{1}^{T}-x_{2})^{T}(x_{1}^{T}-x_{2}^{T})}$$

The corresponding distribution for this kernel is a normal distribution. For more details, refer to Supplementary Info S3. We multiply Q by X and apply a kernel-specific activation function elementwise to generate the "transformed" input matrix Z. For the RBF kernel, for example, the corresponding activation functions are sine and cosine functions (for more details, refer to Supplementary Info S3).

This scheme may be expensive if we need to generate a large number of random features, since random feature generation now scales as O(NDM). We can reduce this cost by adopting the suggestion of Yu et al.²⁹ and replacing the matrix Q with a series of fast transformations. Again, we illustrate using the RBF kernel, where Q can be replaced with:

$$SHD_1HD_2HD_3$$

where S is a diagonal matrix with elements drawn from a χ -distribution with d degrees of freedom, H is the normalized Hadamard matrix, and D_1 , D_2 , D_3 are diagonal matrices with elements drawn from the Rademacher distribution. We can then replace the Hadamard matrix with a fast Hadamard transform³⁰. This reduces the cost of generating the random features to $O(NM \log M)$. We write an implementation of the fast Hadamard transform for CPU and GPU and compare it with matrix multiplication in the Numpy and Cupy libraries under Supplementary Info Section S5. Our implementation is faster for modest numbers of random features, and the performance advantage increases with larger numbers of random features as expected.

Note that some other kernels we implement involve different "recipes" for random feature generation. For all of these, however, we are able to generate random features using fast Hadamard transform based schemes. The polynomial kernel, for example, can be approximated using random features via several different schemes presented in Wacker et al.⁵⁴, including a fast Hadamard transform-based approach. We discuss two others (the neural network kernel and the arccosine kernel) in Supplementary Info Section S3; these as well can be generated using fast Hadamard transform based approaches.

As described under Results, we introduce a novel approach for accelerating a 1d-convolution kernel using the fast Hadamard transform, which we refer to as FHTConv-1d. Note that the 1d-convolution kernel of Morrow et al.³⁸ is merely an approximation to an RBF kernel evaluated pairwise over all pairs of subsequences in the two input sequences. Since

 $e^{-\gamma(x_1-x_2)^T(x_1-x_2)} \approx z(x_1)^T z(x_2)$ using the random features approximation, they approximate this

kernel as $(\sum_{i}^{d-n} z_i)^T (\sum_{j}^{d-n} z_j)$. We see then that this kernel is implemented by applying the random features transformation to the features associated with each subsequence in each input

features transformation to the features associated with each subsequence in each input sequence, which can be implemented as matrix multiplication. Indeed, convolution is often implemented as matrix multiplication in deep learning libraries.

Consider a case where the number of features d associated with each subsequence is a power of 2, which we can trivially achieve by zero padding. We also assume for simplicity that the number of random features desired, m, is the same as d. If m is less than d, we can merely generate d random features and discard the excess; if it is greater, we merely generate d random features x times where x is the result of ceiling division of m by d. Given the above, the cost of the random feature convolution operation scales as $O(NKm^2)$ where K is the number of subsequences in each sequence.

Just as we did for the RBF kernel, we now replace the matrix of convolution filters with the SORF operation:

$$SHD_1HD_2HD_3$$

Where S, D1, D2, D3 are diagonal matrices and H corresponds to the normalized fast Hadamard transform. Because our modification reduces cost from $O(NKM^2)$ to $O(NKM \log M)$, it is faster if the convolution width is large, or the number of features per sequence element is large. Consequently the implementation in xGPR allows the user to prefer FHTConv-1d if there are many features per sequence element or the width of the convolution kernel is large. The reduction in memory footprint is also be dramatic, since we merely store four diagonal matrices, three of which only contain eight-bit integers.

These modifications all improve the speed of random feature generation. The largest cost associated with model fitting, however, is matrix decomposition, which scales with the cube of the number of random features. Recall that the mean of the process (the predicted value) for new datapoints is given as:

$$\mu_* = z_*^T [Z^T Z + \lambda^2 I]^{-1} Z^T y = z_*^T w$$

Where Z is the input matrix transformed as described above, such that row i is $z(x_i)$ and z_i is $z(x_i)$ for new datapoint x_i . It is therefore highly desirable to find iterative methods for fitting the model such that direct matrix decomposition can be avoided. In initial experiments, we sought to use some of the adaptive learning rate stochastic gradient descent methods popular for deep learning (AMSGrad). As illustrated in Figure 1b, however, AMSGrad exhibits poor performance. In initial experiments, Adam and Adadelta, two other popular stochastic gradient descent

methods, were likewise unable to achieve the desired error threshold in under a thousand epochs. It is important to note that the fitting problem is often ill-conditioned, which likely accounts for the poor performance of these stochastic algorithms. The SAG and SAGA stochastic gradient methods are also fairly impractical, since they require storage of a gradient calculated for each datapoint in the training set^{55,56}.

We therefore adopt instead two alternative methods. First, we consider stochastic variance-reduced gradient descent (SVRG)³⁵, in which the high variance of stochastic gradient descent is reduced by using a "snapshot" full gradient acquired on every second epoch. We also consider the method of conjugate gradients³², which achieves the desired subquadratic scaling in the number of random features. Importantly, for either method, on each iteration we can load the data in chunks and process it one chunk at a time. This confers the ability to scale to multiple CPUs / GPUs in a straightforward way and ensures that the cost of one iteration of preconditioned conjugate gradients (PCG) is the same as the cost of one epoch of stochastic gradient descent. There is of course the difference that stochastic gradient descent takes many steps per epoch while PCG takes one. In practice, however, this is not always as significant of an advantage for stochastic gradient descent as it might seem, since SVRG like other stochastic gradient descent methods requires extensive learning rate tuning to achieve a good result, whereas PCG requires no such optimization. We briefly considered the hypergradient descent learning rate update introduced by Baydin et al⁵⁷ but we found that in practice for the problems of interest to us it can sometimes cause unexpected divergence; it therefore lacks the stability and predictability we require for a useful fitting algorithm.

Conjugate gradients solves the system Aw = b for w. It can be shown⁵⁸ that the residual error on iteration n has as its upper bound:

$$2\left(\frac{\sqrt{\kappa-1}}{\sqrt{\kappa+1}}\right)^n||e_0||$$

where κ is the condition number of A, and $||e_0||$ is the error of the initial guess. If κ is large, the algorithm will therefore converge very slowly. A preconditioner whose inverse M^{-1} which is a close approximation to the inverse of A will reduce the condition number of A and accelerate convergence⁵⁸. It is critical for our purposes to have a preconditioner that can be constructed without explicitly forming the matrix Z^TZ , which will require expensive matrix multiplications and for large numbers of random features will be too large to store in memory.

Kernel matrices for Gaussian processes have sometimes been approximated using the Nystrom method (for details, see the Online Methods and Supplementary Info Section S6). In our study, we have instead proposed the use of this method as a preconditioner for a random features approximation of a Gaussian process. This approach has not been used previously for fitting Gaussian processes. In our implementation, for the system:

$$(Z^TZ + \lambda^2 I)^{-1}Z^Ty = w$$

A low-rank approximation of $Z^TZ = A$ is provided by:

$$A_{nystrom} \approx (A\Omega)(\Omega^T A\Omega)^{\dagger}(A\Omega)^T$$

where for Ω we use Q from the QR decomposition of an iid matrix drawn from a zero mean, unit-variance normal distribution; Ω is of size L x M, where M is the number of random features. For an algorithm to construct and use the preconditioner, see the Supplementary Info section S6. In our implementation, we construct the preconditioner using one chunk of the data at a time, so that we never need load the full dataset into memory or construct Z^TZ .

We also implement two modifications which the user can select. The first greatly reduces the cost of constructing the preconditioner. In this modification, rather than constructing it through the matrix multiplication $A\Omega$, we instead use the subsampled randomized Hadamard transform (SRHT). For details of our modified algorithm, refer to the Supplementary Info section S6. This modification replaces matrix multiplication with a fast transform and is close to 2x faster than the traditional approach on GPU even for small datasets; its speed advantage increases for larger datasets or a larger number of random features. The use of the SRHT (or alternatively the subsampled randomized Fourier transform or SRFT) for low-rank matrix approximations was briefly considered by Halko et al. 59, but they concluded that like the subsampled randomized Fourier transform it has worse theoretical guarantees. Remarkably, we found empirically that on our benchmark datasets, a preconditioner constructed using SRHT is not only much faster to build, but provides equal or better acceleration for conjugate gradients in every single case. See the Supplementary Info section S6 for details. We have therefore implemented both approaches to constructing the preconditioner in xGPR with the SRHT-based approach as default in light of its much greater speed and good empirical performance.

As a second modification, we propose constructing a preconditioner using a two-pass method. First, we construct the product $A\Omega$, then use a QR decomposition to produce from this an orthonormal matrix Q. Next we form the product AQ and use this to build the preconditioner. The first pass can be run using the SRHT-based modification described above. This approach requires two passes over the dataset rather than one but it constructs a preconditioner that consistently achieves better performance, reducing the number of iterations required for CG to converge by 25% on average. As illustrated in Figure 1a, the two-pass algorithm ("srht-2") reduces the number of iterations required to reach a fixed tolerance by comparison with the one-pass algorithm ("srht") across a range of datasets and specified rank values. For details and for more performance comparisons with the unmodified randomized Nystrom approximation, refer to the Supplementary Info section S6.

Evaluating xGPR performance: Protein sequences

To evaluate the performance of xGPR on protein engineering-related tasks, we assess its accuracy on tasks from Rao et al. and Dallago et al. 41,42 (the TAPE benchmarks and FLIP benchmarks respectively). We use only tasks that involve regression, since our library does not perform classification at this time. In these comparisons, we *only* use one-hot encoded sequence data as inputs to the GP and *only* compare against deep learning models that are also using one-hot encoded inputs. This is to ensure that we are measuring the performance of the modeling technique and not the selected representation. We tune the hyperparameters in triplicate and fit in triplicate using different random seeds; the resulting error bar measures variability across different random seeds.

For all datasets with the exception of GB1, we use the FHTConv-1d and FastConv-1d kernels that we developed. We report whichever of the two is best in the table; for a full comparison of FHTConv-1d with FastConv-1d, see the Supplementary Info (also Figure 1c). They offer very similar performances. For the GB1 dataset, each sequence is only four amino acids in length,

too short for a convolution kernel to be useful; we therefore use a simple RBF kernel for this dataset instead.

In all cases, the objective is to predict a real-valued property (fitness, fluorescence, binding affinity etc.) of a protein sequence. Performance is assessed using the Spearman-r coefficient. We omit benchmarks from those sources that do not involve regression, involve only a very few training sequences (e.g. < 100), or require extensive extrapolation. We use one-hot encoding for all sequences and tune hyperparameters on the training set by maximizing the marginal likelihood using the 1d matrix decomposition-based Bayesian optimization strategy described under Results using 3,000 random features. Remarkably, we do not need to perform a second round of hyperparameter fine-tuning using a larger number of random features as described in the standard workflow of Figure 2c; the first round of hyperparameter tuning is sufficient to achieve the performance shown here.

We tune in triplicate using three different random seeds to examine the impact of the random seed. We also fit in triplicate using three different random seeds and perform two separate rounds of fitting. In the first round, we fit with 8,192 random features and in the second, we fit with 16,384 random features to examine the impact of random features on performance.

Evaluating xGPR performance: Tabular data

Next, we evaluate xGPR on some large tabular datasets. We use three regression tasks for tabular data benchmarks from Shwartz-Ziv et al.⁴⁴ and Schafl et al.⁴⁵. We do not evaluate on classification tasks since xGPR only performs regression at this time. The deep learning models are DNF-NET⁴⁶, TabNet⁴⁷, a 1d-CNN⁴⁴ and Hopular⁴⁵. It is worthwhile to note that these networks have been specially designed to perform well on tabular data, although as Shwartz-Ziv et al demonstrate, deep learning is in practice often inferior to gradient boosted trees for these types of tasks.

For the first two datasets, there are predefined training and testing sets; we use these and report our results on the test set. For the third dataset, there is no predefined test set, so we report results for a 5x cross validation. We choose a Matern-5/2 kernel as a simple default in all cases, without evaluating any alternatives. We tune hyperparameters using the standard workflow from Figure 2b, in which we first tune using 2,048 random features using our novel Bayesian optimization approach and next "fine-tune" using the approximate marginal likelihood as calculated using 8,192 random features. Finally, we fit using 32,768 random features.

Evaluating xGPR performance: Small molecules

To assess performance on small molecule property prediction, we benchmark on the QM9 dataset of Ramakrishnan et al.⁴⁸, which contains 134,000 small molecules whose geometry has been optimized using density functional theory (DFT). This dataset has been widely used to benchmark models for prediction of energetic & thermodynamic properties and other properties as well. We focus on energetic and thermodynamic properties here since the kernels we have introduced conduct pairwise comparisons over all pairs of atomic environments in two molecules, which suggests they are likely to be useful for properties that can be decomposed into a sum of per-atom contributions.

For an initial evaluation, we one-hot encode each atom and its neighbors sorted by distance, out to the 15th most distant atom (the choice of 15 is arbitrary). We weight each one-hot encoded neighbor by 1 / distance**6; the sixth power is selected here to correspond to the London matrix representation of small molecules⁶⁰. We then use this representation as input to an xGPR model with a GraphConv1d kernel and tune hyperparameters using the standard workflow from Figure

. Using this simple and uninformative representation, which discards all information about bond angles, we are able to quickly achieve a mean absolute error < 1.10 kcal/mol. See the small molecule tutorial in the xGPR documentation for the full results.

Next, we use the smooth overlap of atomic positions (SOAP) features discussed earlier as implemented in the dscribe⁴⁹ library in Python. The SOAP descriptors represent each atom as a Gaussian and expand the resulting density in an orthonormal basis of radial basis functions and spherical harmonics. They have been widely used for predicting energetics and related properties, and they share some similarities with some of the featurizations used for deep learning models trained on this dataset.

The larger the number of basis functions used for generating the SOAP descriptor, the more accurate the representation, which generally increases the accuracy of the GP⁶¹. Increasing the number of basis functions however makes the descriptor vector much larger. We use 12 radial basis functions and 9 spherical harmonics, which already results in roughly 18,000 features per atom! This large feature vector slows down fitting since each "chunk" of data that must be loaded into memory when looping over the dataset is quite large. Reducing the size of the descriptor vector would significantly reduce computational expense and enable us to use more basis functions to increase accuracy. There are several recent proposals in the literature for similar representations that are significantly more compact and yet achieve similar performance^{62–64} Choosing one of these is beyond the scope of this study, so for the time being we use the SOAP descriptors "as-is" and defer their improvement to future work.

The SOAP descriptors have several hyperparameters that must be optimized. We start from settings selected by Willat et al. and perform some further limited optimization on a random sample of the training data (25,000 datapoints) and by comparing the marginal likelihood for the GP model for internal energy *only* with different hyperparameter settings. This is an efficient approach to feature engineering since each experiment only requires hyperparameter tuning with a small number of random features (2,048) on a small subset of the training data. For additional details, see the Supplementary Info section S12.

The kernel hyperparameters are tuned using the standard workflow in Figure 2c. We first tune using the matrix decomposition-based Bayesian strategy for a smaller number of random features, then "fine-tune" using Bayesian optimization with approximate marginal likelihood with 16,384 random features. We tune hyperparameters using the energy at 298K as an objective only. Like other authors, we randomly divide the dataset (using random seed 123) into a training set of 110,000 datapoints, a validation set of 10,000 datapoints and the remaining points (a little over 10,000) as test set. We fit using either 16,384, 32,768 or 65,536 random features to explore how performance changes as the number of random features increases.

REFERENCES

- Lutz, S. & Iamurri, S. M. Protein Engineering: Past, Present, and Future. in *Protein Engineering* (eds. Bornscheuer, U. T. & Höhne, M.) vol. 1685 1–12 (Springer New York, 2018).
- 2. Frappier, V. & Keating, A. E. Data-driven computational protein design. *Curr. Opin. Struct. Biol.* **69**, 63–69 (2021).
- 3. Luo, Y. *et al.* ECNet is an evolutionary context-integrated deep learning framework for protein engineering. *Nat. Commun.* **12**, 5743 (2021).
- 4. Notin, P. *et al.* Tranception: protein fitness prediction with autoregressive transformers and inference-time retrieval. Preprint at https://doi.org/10.48550/arXiv.2205.13760 (2022).
- 5. Yang, K. K., Wu, Z. & Arnold, F. H. Machine-learning-guided directed evolution for protein engineering. *Nat. Methods* **16**, 687–694 (2019).
- 6. Bepler, T. & Berger, B. Learning the protein language: Evolution, structure, and function. *Cell Syst.* **12**, 654-669.e3 (2021).
- 7. Liu, G. *et al.* Antibody complementarity determining region design using high-capacity machine learning. *Bioinformatics* **36**, 2126–2133 (2020).
- 8. Mason, D. M. *et al.* Optimization of therapeutic antibodies by predicting antigen specificity from antibody sequence via deep learning. *Nat. Biomed. Eng.* **5**, 600–612 (2021).
- Parkinson, J., DeCastro, J. H., Goldsmith, B. & Aran, K. Machine Learning for Disease Classification: A Perspective. in *Artificial Intelligence in Healthcare and Medicine* (CRC Press, 2022).
- 10. Gawlikowski, J. *et al.* A Survey of Uncertainty in Deep Neural Networks. Preprint at https://doi.org/10.48550/arXiv.2107.03342 (2022).
- 11. Blundell, C., Cornebise, J., Kavukcuoglu, K. & Wierstra, D. Weight Uncertainty in Neural Networks. *ArXiv150505424 Cs Stat* (2015).
- 12. Angelopoulos, A. N. & Bates, S. A Gentle Introduction to Conformal Prediction and

- Distribution-Free Uncertainty Quantification. Preprint at https://doi.org/10.48550/arXiv.2107.07511 (2022).
- 'In-Between' Uncertainty in Bayesian Neural Networks. *DeepAI* https://deepai.org/publication/in-between-uncertainty-in-bayesian-neural-networks (2019).
- 14. Ilyas, A., Engstrom, L., Athalye, A. & Lin, J. Black-box Adversarial Attacks with Limited Queries and Information. Preprint at http://arxiv.org/abs/1804.08598 (2018).
- 15. Jha, S. K., Ramanathan, A., Ewetz, R., Velasquez, A. & Jha, S. *Protein Folding Neural Networks Are Not Robust*. http://arxiv.org/abs/2109.04460 (2021) doi:10.48550/arXiv.2109.04460.
- Xu, R. et al. From Dense to Sparse: Contrastive Pruning for Better Pre-trained Language
 Model Compression. Preprint at http://arxiv.org/abs/2112.07198 (2021).
- 17. Rasmussen, C. & Williams, C. Gaussian Processes for Machine Learning. Vol. 2. No. 3. Cambridge, MA: MIT press, 2006. vol. 2 (MIT Press, 2006).
- 18. Koh, P. W. *et al.* WILDS: A Benchmark of in-the-Wild Distribution Shifts. in *Proceedings of the 38th International Conference on Machine Learning* 5637–5664 (PMLR, 2021).
- Taori, R. et al. Measuring Robustness to Natural Distribution Shifts in Image Classification. in Advances in Neural Information Processing Systems vol. 33 18583–18599 (Curran Associates, Inc., 2020).
- DeGrave, A. J., Janizek, J. D. & Lee, S.-I. Al for radiographic COVID-19 detection selects shortcuts over signal. *medRxiv* 2020.09.13.20193565 (2020) doi:10.1101/2020.09.13.20193565.
- Roberts, M. et al. Common pitfalls and recommendations for using machine learning to detect and prognosticate for COVID-19 using chest radiographs and CT scans. *Nat. Mach. Intell.* 3, 199–217 (2021).
- 22. Gardner, J. R., Pleiss, G., Bindel, D., Weinberger, K. Q. & Wilson, A. G. GPyTorch: Blackbox Matrix-Matrix Gaussian Process Inference with GPU Acceleration. Preprint at

- https://doi.org/10.48550/arXiv.1809.11165 (2021).
- 23. Li, Y., Yu, R., Shahabi, C. & Liu, Y. Diffusion Convolutional Recurrent Neural Network:

 Data-Driven Traffic Forecasting. Preprint at http://arxiv.org/abs/1707.01926 (2018).
- 24. Kriege, N. M., Johansson, F. D. & Morris, C. A Survey on Graph Kernels. *Appl. Netw. Sci.* **5**, 6 (2020).
- 25. Nguyen, T. & Bonilla, E. Fast Allocation of Gaussian Process Experts. in *Proceedings of the*31st International Conference on Machine Learning 145–153 (PMLR, 2014).
- 26. Hensman, J., Fusi, N. & Lawrence, N. D. Gaussian Processes for Big Data. (2013).
- Bauer, M., van der Wilk, M. & Rasmussen, C. E. Understanding Probabilistic Sparse
 Gaussian Process Approximations. in *Advances in Neural Information Processing Systems* vol. 29 (Curran Associates, Inc., 2016).
- 28. Rahimi, A. & Recht, B. Random features for large-scale kernel machines. in *In Advances in Neural Information Processing Systems (nips* (2007).
- Yu, F. X. X., Suresh, A. T., Choromanski, K. M., Holtmann-Rice, D. N. & Kumar, S.
 Orthogonal Random Features. in *Advances in Neural Information Processing Systems* vol.
 (Curran Associates, Inc., 2016).
- 30. Fino & Algazi. Unified Matrix Treatment of the Fast Walsh-Hadamard Transform. *IEEE Trans. Comput.* **C–25**, 1142–1146 (1976).
- 31. Iterative Solution of Large Sparse Systems of Equations.
- 32. Saad, Y. *Iterative Methods for Sparse Linear Systems*. (Society for Industrial and Applied Mathematics, 2003). doi:10.1137/1.9780898718003.
- 33. Alaoui, A. & Mahoney, M. W. Fast Randomized Kernel Ridge Regression with Statistical Guarantees. in *Advances in Neural Information Processing Systems* vol. 28 (Curran Associates, Inc., 2015).
- 34. Nocedal, J. & Wright, S. Numerical Optimization. (Springer Science+Business Media, 2006).
- 35. Johnson, R. & Zhang, T. Accelerating Stochastic Gradient Descent using Predictive

- Variance Reduction. in *Advances in Neural Information Processing Systems* vol. 26 (Curran Associates, Inc., 2013).
- Frazier, P. I. A Tutorial on Bayesian Optimization. Preprint at https://doi.org/10.48550/arXiv.1807.02811 (2018).
- 37. Ubaru, S., Chen, J. & Saad, Y. Fast Estimation of \$tr(f(A))\$ via Stochastic Lanczos Quadrature. *SIAM J. Matrix Anal. Appl.* **38**, 1075–1099 (2017).
- 38. Morrow, A. *et al.* Convolutional Kitchen Sinks for Transcription Factor Binding Site Prediction. Preprint at https://doi.org/10.48550/arXiv.1706.00125 (2017).
- 39. Choromanski, K. *et al.* The Geometry of Random Features. in *Proceedings of the Twenty-First International Conference on Artificial Intelligence and Statistics* 1–9 (PMLR, 2018).
- 40. Bartók, A. P., Kondor, R. & Csányi, G. On representing chemical environments. *Phys. Rev. B* **87**, 184115 (2013).
- 41. Rao, R. *et al.* Evaluating Protein Transfer Learning with TAPE. *ArXiv190608230 Cs Q-Bio Stat* (2019).
- 42. Dallago, C. *et al.* FLIP: Benchmark tasks in fitness landscape inference for proteins. *Proc.*Neural Inf. Process. Syst. Track Datasets Benchmarks 1, (2021).
- 43. Detlefsen, N. S., Hauberg, S. & Boomsma, W. Learning meaningful representations of protein sequences. *Nat. Commun.* **13**, 1914 (2022).
- 44. Shwartz-Ziv, R. & Armon, A. Tabular Data: Deep Learning is Not All You Need. Preprint at https://doi.org/10.48550/arXiv.2106.03253 (2021).
- 45. Schäfl, B., Gruber, L., Bitto-Nemling, A. & Hochreiter, S. Hopular: Modern Hopfield Networks for Tabular Data. Preprint at https://doi.org/10.48550/arXiv.2206.00664 (2022).
- 46. Li, X., Li, R., Zhu, L., Fu, C.-W. & Heng, P.-A. DNF-Net: A Deep Normal Filtering Network for Mesh Denoising. *IEEE Trans. Vis. Comput. Graph.* **27**, 4060–4072 (2021).
- 47. Arik, S. O. & Pfister, T. TabNet: Attentive Interpretable Tabular Learning. Preprint at

- https://doi.org/10.48550/arXiv.1908.07442 (2020).
- 48. Ramakrishnan, R., Dral, P. O., Rupp, M. & von Lilienfeld, O. A. Quantum chemistry structures and properties of 134 kilo molecules. *Sci. Data* **1**, 140022 (2014).
- 49. Himanen, L. *et al.* DScribe: Library of descriptors for machine learning in materials science. *Comput. Phys. Commun.* **247**, 106949 (2020).
- 50. Ullah, E., Mianjy, P., Marinov, T. V. & Arora, R. Streaming Kernel PCA with \$\tilde{O}(\sqrt{n})\$ Random Features. Preprint at https://doi.org/10.48550/arXiv.1808.00934 (2018).
- Chitta, R., Jin, R. & Jain, A. K. Efficient Kernel Clustering Using Random Fourier Features.
 in *Proceedings of the 2012 IEEE 12th International Conference on Data Mining* 161–170
 (IEEE Computer Society, 2012). doi:10.1109/ICDM.2012.61.
- Milios, D., Camoriano, R., Michiardi, P., Rosasco, L. & Filippone, M. Dirichlet-based Gaussian Processes for Large-scale Calibrated Classification. Preprint at https://doi.org/10.48550/arXiv.1805.10915 (2018).
- 53. Willatt, M. J., Musil, F. & Ceriotti, M. Feature Optimization for Atomistic Machine Learning Yields A Data-Driven Construction of the Periodic Table of the Elements. *Phys. Chem. Chem. Phys.* 20, 29661–29668 (2018).
- 54. Wacker, J., Ohana, R. & Filippone, M. Complex-to-Real Random Features for Polynomial Kernels. Preprint at https://doi.org/10.48550/arXiv.2202.02031 (2022).
- 55. Defazio, A., Bach, F. & Lacoste-Julien, S. SAGA: A Fast Incremental Gradient Method With Support for Non-Strongly Convex Composite Objectives. Preprint at http://arxiv.org/abs/1407.0202 (2014).
- 56. Schmidt, M., Roux, N. L. & Bach, F. Minimizing Finite Sums with the Stochastic Average Gradient. Preprint at https://doi.org/10.48550/arXiv.1309.2388 (2016).
- 57. Baydin, A. G., Cornish, R., Rubio, D. M., Schmidt, M. & Wood, F. Online Learning Rate

 Adaptation with Hypergradient Descent. Preprint at

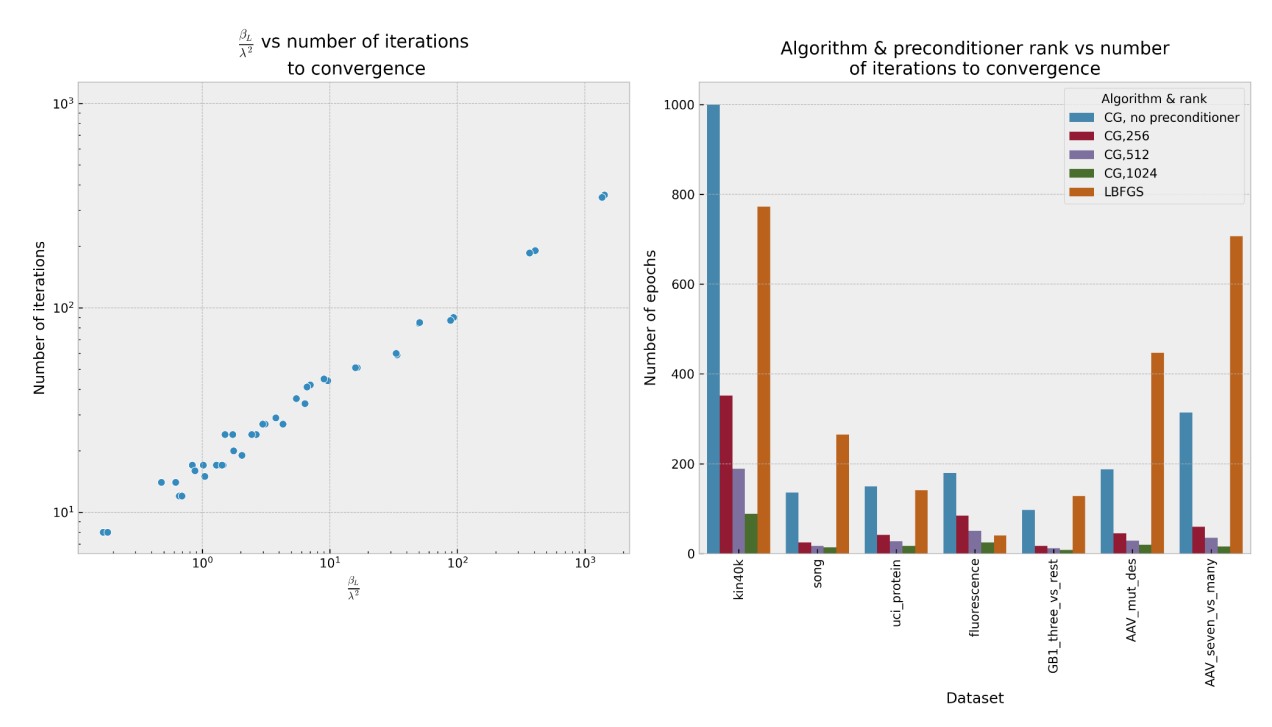
- https://doi.org/10.48550/arXiv.1703.04782 (2018).
- 6. Krylov Subspace Methods, Part I. in *Iterative Methods for Sparse Linear Systems* 151–216 (Society for Industrial and Applied Mathematics, 2003).
 doi:10.1137/1.9780898718003.ch6.
- Halko, N., Martinsson, P.-G. & Tropp, J. A. Finding structure with randomness: Probabilistic algorithms for constructing approximate matrix decompositions. Preprint at http://arxiv.org/abs/0909.4061 (2010).
- Huang, B. & von Lilienfeld, O. A. Communication: Understanding molecular representations in machine learning: The role of uniqueness and target similarity. *J. Chem. Phys.* 145, 161102 (2016).
- 61. Bartók, A. P. *et al.* Machine learning unifies the modeling of materials and molecules. *Sci. Adv.* **3**, e1701816 (2017).
- 62. Darby, J. P., Kermode, J. R. & Csányi, G. Compressing local atomic neighbourhood descriptors. *Npj Comput. Mater.* **8**, 1–13 (2022).
- 63. Onat, B., Ortner, C. & Kermode, J. R. Sensitivity and dimensionality of atomic environment representations used for machine learning interatomic potentials. *J. Chem. Phys.* **153**, 144106 (2020).
- 64. Kocer, E., Mason, J. K. & Erturk, H. Continuous and optimally complete description of chemical environments using Spherical Bessel descriptors. *AIP Adv.* **10**, 015021 (2020).
- 65. Wu, Z. *et al.* MoleculeNet: A Benchmark for Molecular Machine Learning. Preprint at http://arxiv.org/abs/1703.00564 (2018).
- 66. Jørgensen, P. B., Jacobsen, K. W. & Schmidt, M. N. Neural Message Passing with Edge Updates for Predicting Properties of Molecules and Materials. Preprint at https://doi.org/10.48550/arXiv.1806.03146 (2018).
- 67. Gilmer, J., Schoenholz, S. S., Riley, P. F., Vinyals, O. & Dahl, G. E. Neural Message Passing for Quantum Chemistry. *ArXiv170401212 Cs* (2017).

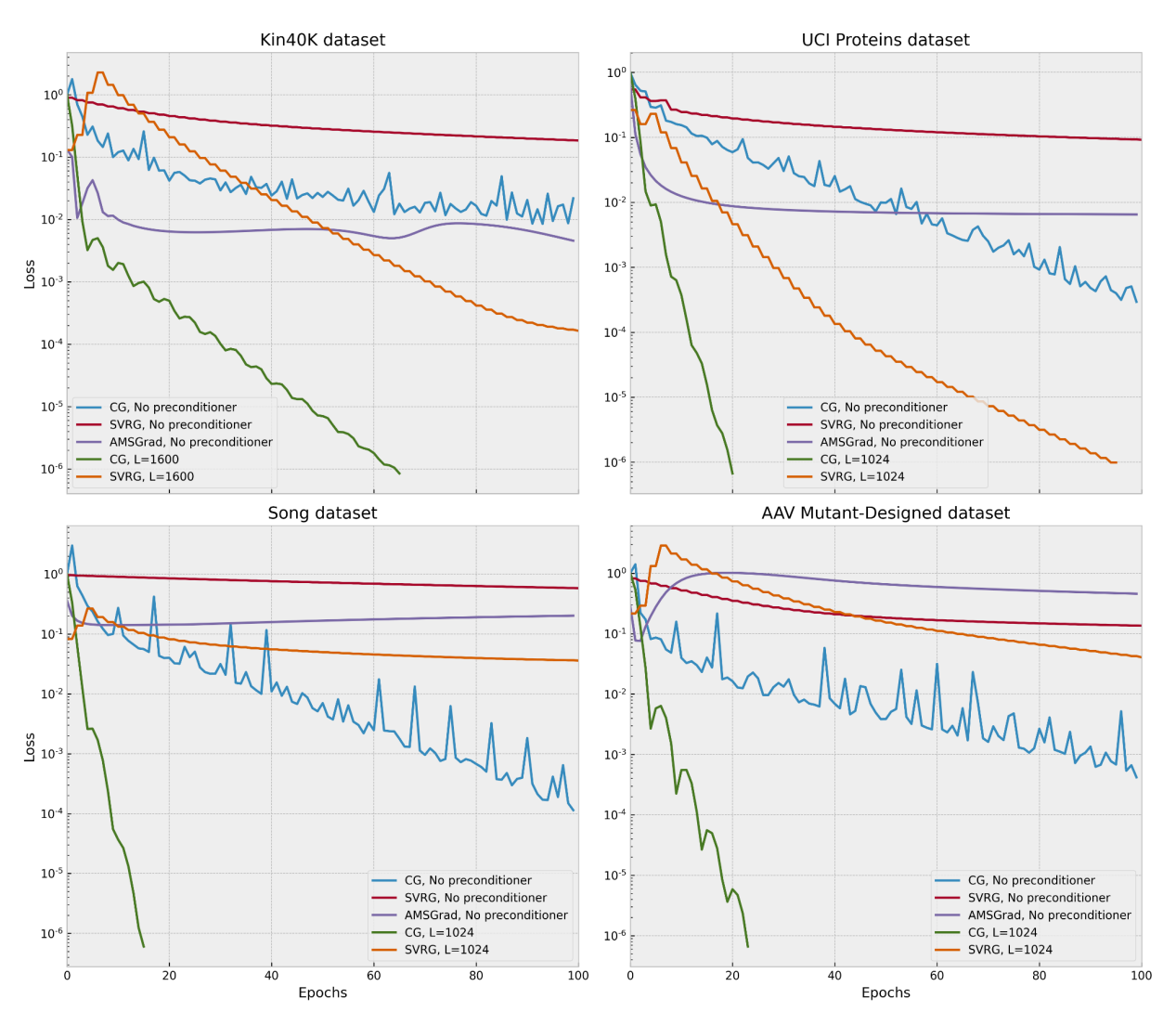
- 68. Schütt, K. T., Sauceda, H. E., Kindermans, P.-J., Tkatchenko, A. & Müller, K.-R. SchNet A deep learning architecture for molecules and materials. *J. Chem. Phys.* **148**, 241722 (2018).
- 69. Anderson, B., Hy, T.-S. & Kondor, R. Cormorant: Covariant Molecular Neural Networks. Preprint at https://doi.org/10.48550/arXiv.1906.04015 (2019).
- 70. Unke, O. T. & Meuwly, M. PhysNet: A Neural Network for Predicting Energies, Forces, Dipole Moments, and Partial Charges. *J. Chem. Theory Comput.* **15**, 3678–3693 (2019).
- 71. Gasteiger, J., Groß, J. & Günnemann, S. Directional Message Passing for Molecular Graphs. Preprint at https://doi.org/10.48550/arXiv.2003.03123 (2022).
- 72. Shui, Z. & Karypis, G. Heterogeneous Molecular Graph Neural Networks for Predicting Molecule Properties. Preprint at https://doi.org/10.48550/arXiv.2009.12710 (2020).
- 73. Wu, F. *et al.* Molformer: Motif-based Transformer on 3D Heterogeneous Molecular Graphs. Preprint at http://arxiv.org/abs/2110.01191 (2022).
- Schütt, K. T., Unke, O. T. & Gastegger, M. Equivariant message passing for the prediction of tensorial properties and molecular spectra. Preprint at http://arxiv.org/abs/2102.03150 (2021).

Figure 1

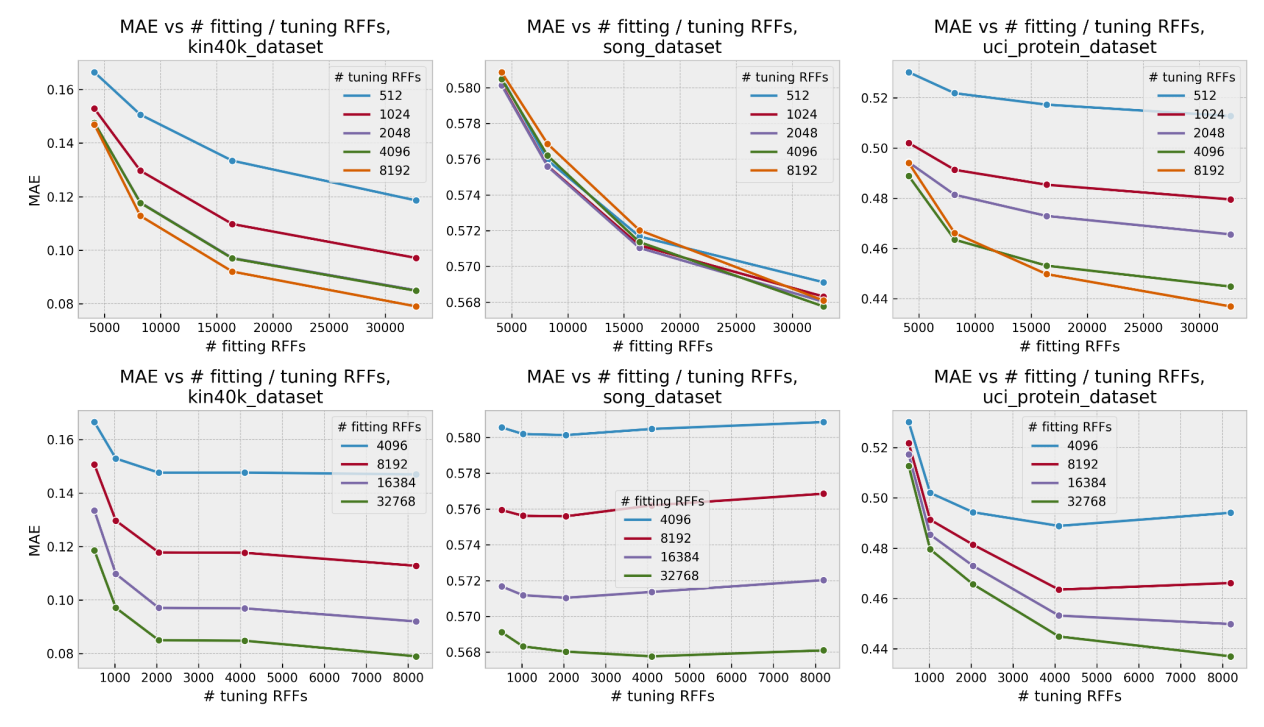
- a. Number of iterations required for conjugate gradients to fit using a threshold of 1e-6 vs the minimum eigenvalue of the preconditioner divided by the "noise" hyperparameter of the kernel on the left. As illustrated, the number of iterations required to fit for a given error threshold can be approximately predicted using this ratio once the preconditioner has been constructed. On the right, preconditioner rank vs number of iterations to reach error of 1e-6 for conjugate gradients, together with number of iterations to convergence for Scipy's implementation of L-BFGS with a threshold of 1e-6.
- b. The error per epoch for conjugate gradients with and without preconditioning vs AMSGrad (a state of the art stochastic gradient descent method) and minibatch SVRG (stochastic variance-reduced gradient descent) with and without preconditioning.
- c. Performance on UCI machine learning datasets as a function of the number of random features used for hyperparameter tuning and for fitting. First row: # fitting RFFs on x-axis, hue indicates # tuning RFFs. Second row: # tuning RFFs on x-axis, hue indicates # fitting RFFs.
- d. Performance for three convolution kernels; hyperparameter tuning time for FastConv-1d divided by hyperparameter tuning time for Conv-1d as a function of the number of training datapoints. Error bars reflect error across tuning hyperparameters and fitting with different random seeds. We observe that for these datasets, FHTConv-1d and Conv-1d achieve very similar if not identical performance. FastConv-1d is also generally similar but in some cases diverges sharply from the other two, especially on smaller datasets (two vs many, one vs many). As illustrated on the right, for large datasets it can be significantly faster.

Α





С





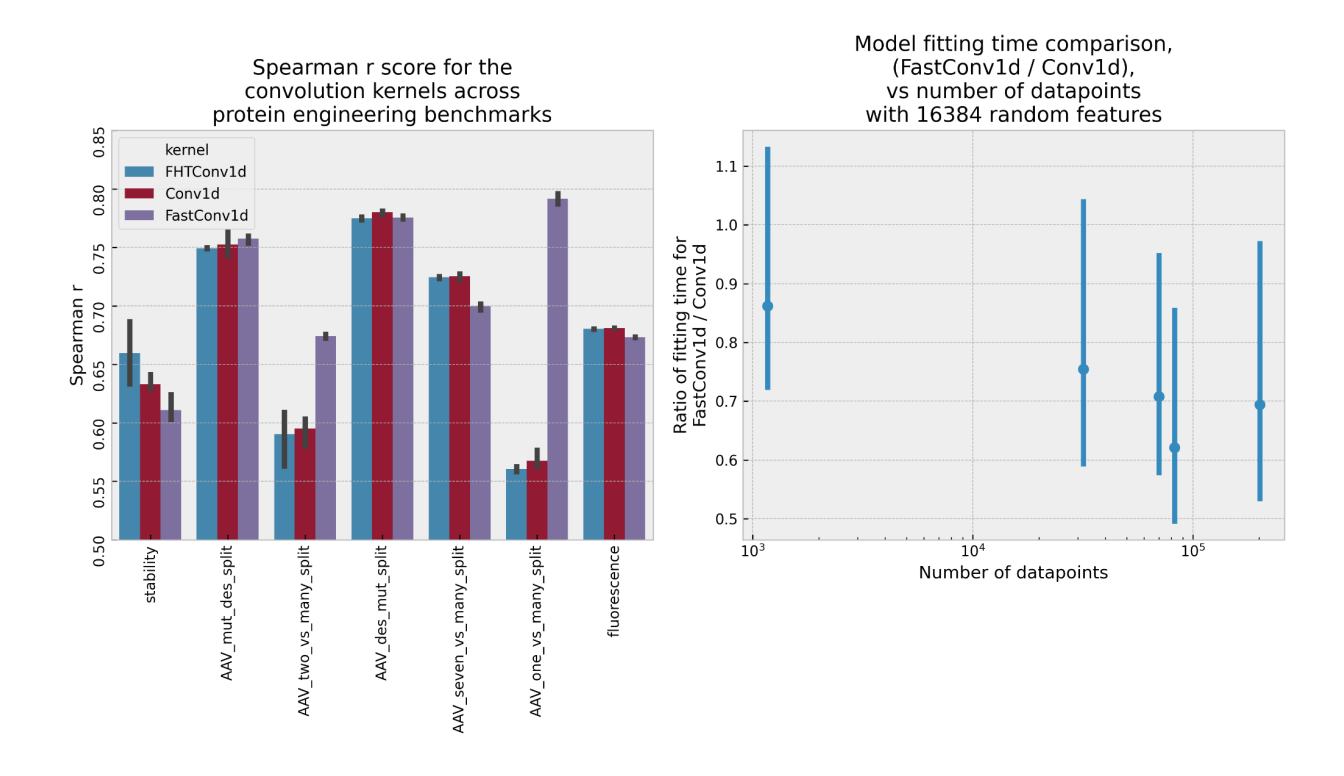
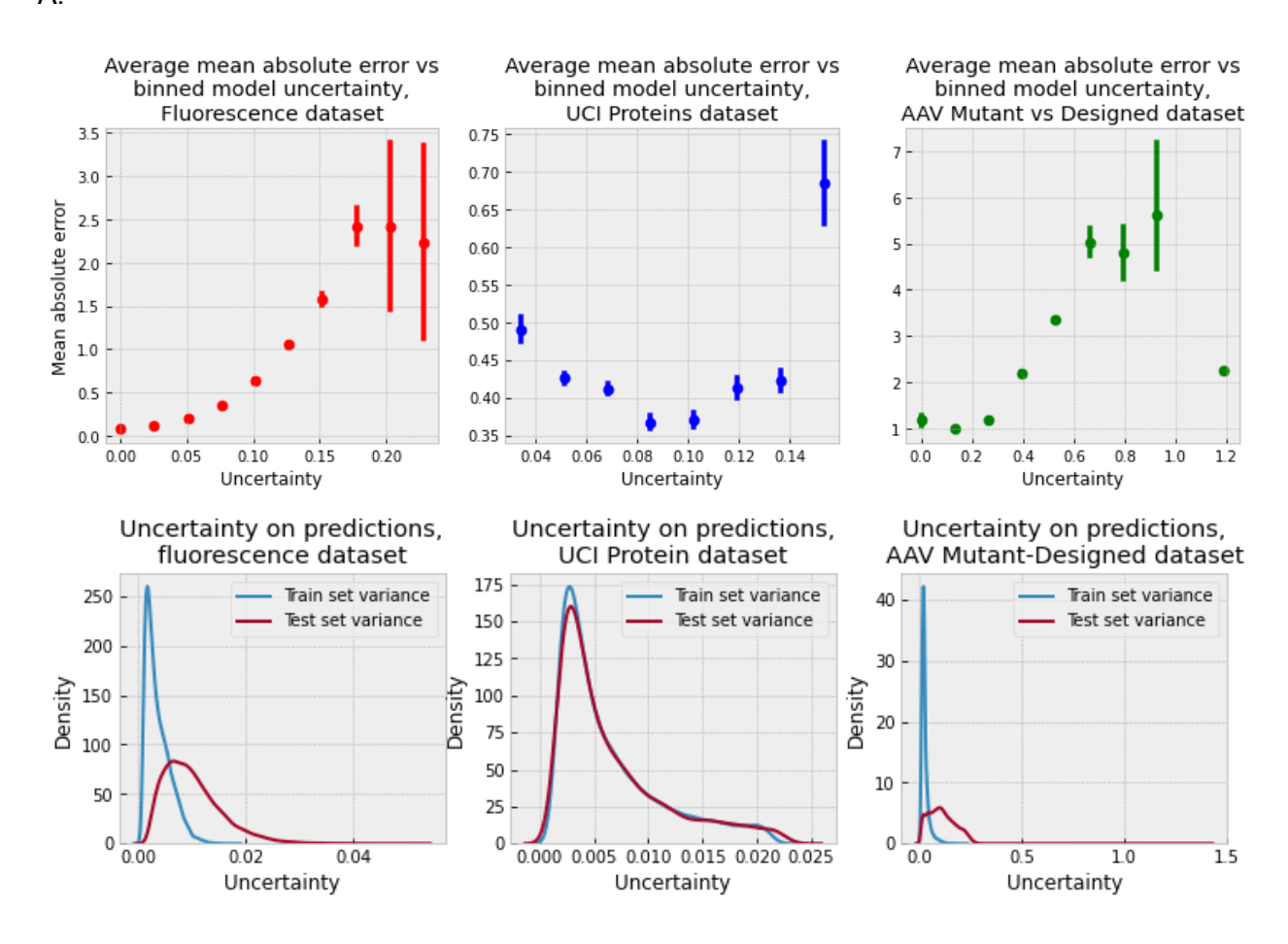


Figure 2

- Mean absolute error vs model uncertainty on training & test set predictions; distribution
 of uncertainty for training and test sets.
- b. Overall xGPR decision tree & workflow.

A.



B.

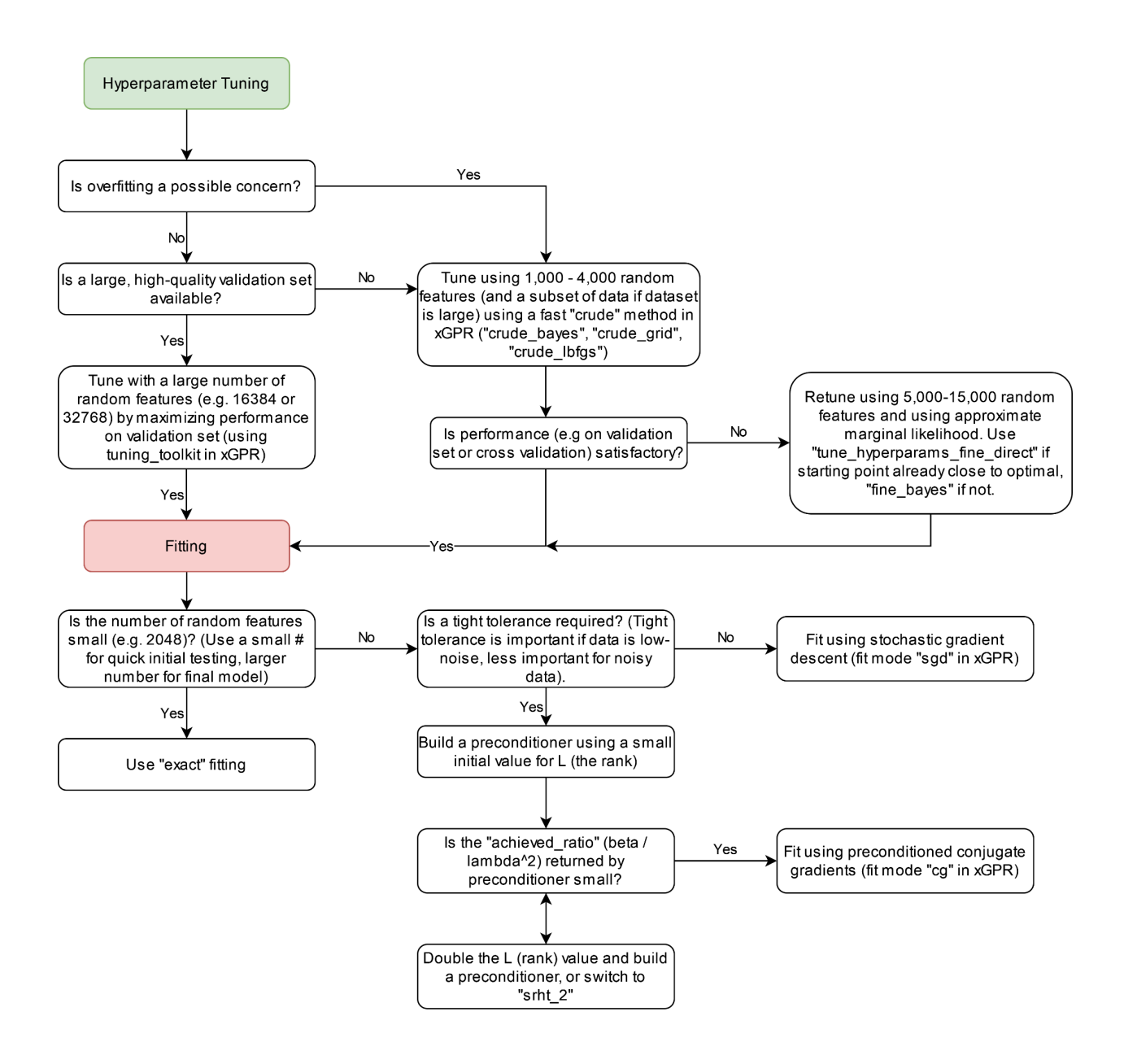


Table 1: Best "score" or negative marginal log likelihood (lower is better) and number of effective iterations (passes over the dataset) for various algorithms for hyperparameter

tuning on selected datasets.

otou dataotti.							
Dataset	L-BFGS		Bayesian Optimization				
	# effective iterations	Best score	# effective iterations	Best score			
UCI Kin40K	91	20188	18	20190			
YearPrediction / Song	16	519537	132	519532			
UCI Protein	16	41057	93	41057			
GB1, 3 vs rest	17	2806	115	2806			
AAV, mutant designed split	19	70331	121	70331			

Table 2. Comparison of GP models with convolutional neural networks protein

engineering benchmarks using one-hot encoding.

Dataset	Split ^a	Data type	# training / test datapoints	Deep learning architecture	Spearman's-r for deep learning model trained on one-hot data	Source	Selected kernel / Spearman's-R for selected kernel with 8,192 random features ^b	Spearman's-R for selected kernel with 16,384 random features
Stability	Stability	Zero-padde d, unaligned	53,614 / 12,581	Convolutional neural net	0.51	Dallago et al	FHTConv1d / 0.610 +/- 0.01	0.660 +/- 0.02
Thermostabilit y	Mixed	Zero-padde d, unaligned	24,817 / 3,134	Convolutional neural net	0.34	Dallago et al	FastConv / 0.351 +/- 0.003	0.366 +/- 0.003
Thermostabilit y	Human only	Zero-padde d, unaligned	8,148 / 1,945	Convolutional neural net	0.5	Dallago et al	FastConv / 0.553 +/- 0.002	0.564 +/- 0.002
Alpha adenovirus (AAV)	Designe d vs mutant	Zero-padde d, unaligned	201,426 / 82,583	Convolutional neural net	0.75	Dallago et al	FHTConv1d / 0.764 +/- 0.002	0.775 +/- 0.0008
Alpha adenovirus (AAV)	Mutant vs designe d	Zero-padde d, unaligned	82,583 / 201,426	Convolutional neural net	0.71	Dallago et al	FastConv / 0.747 +/- 0.004	0.757 +/- 0.002
Alpha adenovirus (AAV)	7 mutation s vs many	Zero-padde d, unaligned	70,002 / 12,581	Convolutional neural net	0.74	Dallago et al	FHTConv-1d / 0.712 +/- 0.001	0.724 +/- 0.0006
Alpha adenovirus (AAV)	2 mutation s vs many	Zero-padde d, unaligned	31,807 / 50,776	Convolutional neural net	0.74	Dallago et al	FastConv / 0.658 +/- 0.004	0.674 +/- 0.001
Alpha adenovirus (AAV)	1 mutation vs many	Zero-padde d, unaligned	1,170 / 81,413	Convolutional neural net	0.48	Dallago et al	FastConv / 0.760 +/- 0.002	0.780 +/- 0.001
GB1	3 vs rest	MSA	2,968 / 5,765	Convolutional neural net	0.83	Dallago et al	RBF 0.821 +/- 0.001	0.827 +/- 0.001
GB1	2 vs rest	MSA	427 / 8,306	Convolutional neural net	0.32	Dallago et al	RBF / 0.624 +/- 0.01	0.623 +/- 0.003
Fluorescence	Fluoresc ence	MSA	21,446 / 27,217	Convolutional neural net	0.68	Rao et al	FHTConv1d / 0.678 +/- 0.0002	0.680 +/- 0.0001

^{a.} In many cases, there are multiple "splits" for the same dataset; for the AAV dataset, for example, the "designed vs mutant" split uses designed sequences as a training set and mutants as test, while the "mutant vs designed" split is the reverse. ^b All convolution kernels use convolution filters of width 9 as a simple default. The best performer for each benchmark is highlighted in bold. If the sequences come as an alignment (so that they are all fixed-length vectors), we select either the RBF kernel or our novel FastConv kernel using marginal likelihood on the training set. If the sequences are not aligned, we use FastConv only. For all the models, we repeat the predictions using three different seeds for the random

number generator, higher is better.	then report the	mean and standa	ard error of the m	nean. For the score	s shown here,

Table 3. Comparison with deep learning and XGBoost on tabular data regression tasks

Dataset	Total datapoints	Metric	XGBoost	DNF-NET	NODE ^a	TabNet ^a	1D-CNN	Hopular NN ^a	xGPR, Matern kernel
Rossman Store Sales	1,018,000	RMSE	490.18 ± 1.19	503.83 ± 1.41	488.59 ± 1.24	485.12±1.93	493.81 ± 2.23		485.9
YearPredictio n (Song)	515,000	MSE	77.98 ± 0.11	81.21 ± 0.18	76.39 ± 0.13	83.19 ± 0.19	78.94 ± 0.14		77.9
Sulfur	10,082	1,000 * MSE	1.23 ± 0.00					1.04 ± 0.02	0.93 +/- 0.07

a. DNF-Net, NODE, TabNet and Hopular are deep learning models designed specifically to perform well on tabular data.

The Rossman Store Sales dataset originated with a 2015 Kaggle competition; the goal is to predict daily sales for specific stores. The YearPrediction dataset requires us to predict the year in which a song was released based on features of the song, and the Sulfur dataset entails prediction of hydrogen sulfide concentrations based on sensor data.

Table 4. Comparison with state of the art deep learning models for prediction of energetic

and thermodynamic properties of small molecules, QM9 dataset

Model	U 0K MAE, kcal/mol	U 298K MAE, kcal/mol	H 298K MAE, kcal/mol	G 298K MAE, kcal/molf	Cv 298K, mol/cal * k	ZPVE, kcal/mol
MPNN ⁶⁵ (deep learning)	2.05	2.00	2.02	2.43	0.42	
DTNN ⁶⁵ (deep learning)	2.43	2.43	2.43	2.02	0.27	
Cormorant ⁶⁹ (deep learning)	0.484	0.507	0.484	0.461	0.026	0.047
Enn-s2s ⁶⁷ (deep learning)	0.44	0.44	0.39	0.44	0.04	0.035
SchNet ⁶⁸ (deep learning)	0.323	0.438	0.323	0.323	0.033	0.039
NMP-EDGE ⁶⁶ (deep learning)	0.242	0.244	0.261	0.281	0.032	0.034
PhysNet ⁷⁰ (deep learning)	0.188	0.189	0.194	0.217	0.028	0.032
DIME ⁷¹ (deep learning)	0.185	0.182	0.187	0.207	0.025	0.030
Molformer ⁷³ (deep learning)	0.173	0.172	0.170	0.169	0.025	0.047
HMGNN ⁷² (deep learning)	0.137	0.158	0.14	0.175	0.023	0.027
PAiNN ⁷⁴ (deep learning)	0.135	0.134	0.138	0.187	0.024	0.030
xGPR, GraphConv1d, 16,384 random features	0.232	0.233	0.233	0.25	0.026	0.029
xGPR, GraphConv1d, 32,768 random features	0.184	0.182	0.188	0.21	0.024	0.027
xGPR, GraphConv1d, 66,536 random features	0.167	0.168	0.166	0.188	0.22	0.027
Exact GP, radially scaled polynomial kernel ⁵³		0.14				

Scalable Gaussian progress regression enables accurate prediction of protein properties with uncertainty quantitation

SUPPLEMENTARY INFO

S1. Datasets used for experiments described in the main text

All datasets used in the paper are publicly available. Details of each dataset are described in the following Table S1.

Table S1. Details of datasets used for experiments in the main text

Dataset name	Data type	Number of datapoints	Task	Link	Citation
UCI SONG	Tabular data	515,345	Predict the year in which a song was released based on features of the song.	https://archive.ics.uci.edu/ml/ datasets/yearpredictionmsd	Bertin-Mahieux et al. ¹
Rossman dataset	Tabular data	1,017,210	From a Kaggle competition: predict store sales based on various characteristics of the store	https://www.kaggle.com/c/ro ssmann-store-sales	No associated paper
Sulfur dataset	Tabular data	10,082	Predict H2S concentrations based on sensor measurements	https://github.com/ml-jku/hop ular/tree/main/hopular/auxilia ry/resources/sulfur	Schafl et al.
UCI Proteins	Tabular data	45,730	Predict the RMSD of a residue based on physicochemical properties.	https://archive.ics.uci.edu/ml/ datasets/Physicochemical+P roperties+of+Protein+Tertiar y+Structure	Qian and Sejnowski 1988.²
UCI Kin40K	Tabular data	40,000	Predict the forward motion of a robot arm using 8 inputs	https://www.cs.utoronto.ca/~ delve/data/kin/desc.html	Corke 1996. ³
Alpha adenovirus (AAV)	Sequence data	201,426	Predict fitness properties of mutant sequences of the AAV capsid protein	https://benchmark.protein.pr operties/landscapes	Dallago et al. ⁴
GB1	Sequence data	8,733	Predict fitness properties of mutants of the binding domain of protein G from Streptococcus	https://benchmark.protein.pr operties/landscapes	Dallago et al. ⁴
Thermostability	Sequence data	27,951	Predict thermostability of a diverse array of proteins from different families	https://benchmark.protein.pr operties/landscapes	Dallago et al. ⁴
Fluorescence	Sequence data	54,025	Predict fluorescence of mutants of GFP	https://github.com/songlab-c al/tape	Rao et al.⁵

Stability	Sequence data	68,965	Predict thermostability of mutant protein sequences. (This is completely unrelated to the thermostability dataset of Dallago et al and is significantly less diverse.)	https://github.com/songlab-c al/tape	Rao et al.⁵
QM9	Graph / small molecule data	134,000	Predict DFT-calculated properties of small molecules given the DFT-optimized gas-phase geometry	https://figshare.com/collectio ns/Quantum_chemistry_stru ctures_and_properties_of_1 34_kilo_molecules/978904	Ramakrishnan et al. ⁶

S2. Comparison of Gaussian process approximations

The stochastic variational approximation to Gaussian process models and variants have appeared frequently in the literature^{7,8}. From a theoretical standpoint it has many attractive properties, but how does it perform in practice? In Table S1, we compare the performance of SVGP as implemented in the GPyTorch library with the random feature approximation as implemented in xGPR; for sufficiently small datasets, we compare also with an exact Gaussian process as implemented in the scikit-learn library. We train GPyTorch for 40 epochs in all cases, and we use the RBF kernel in all cases, since we are not aware of an SVGP-compatible convolution kernel for sequence data sufficiently efficient that we can use it on a > 100,000 sequence dataset in a short period of time, nor are any such kernels implemented in GPyTorch. Training for 20 epochs yielded worse performance in every case.

For xGPR, we tune hyperparameters using 3,000 random features without performing any further "fine-tuning". We then fit using either 16,384 or 32,768 random features for tabular data and 8,192 or 16,384 random features for sequence data (we use a smaller number of random features for sequence data to correspond to the number of features used for comparison with CNN deep learning models on sequence data in the main text). As discussed and demonstrated in the main text, we can easily "fine-tune" hyperparameters using a larger number of random features to achieve further improved performance.

Table S1 clearly shows that xGPR outperforms SVGP on 8 out of 9 datasets, often by large margins. In the case where SVGP is competitive (Song UCI), they achieve essentially equivalent performance, and SVGP takes eighty times longer to train. xGPR generally performs better using the same kernel and at greatly reduced cost; moreover, performance for xGPR can often be further improved by either using more random features for fitting, or by fine-tuning hyperparameters with a larger number of random features, both using highly scalable procedures as described in the main text. On the Kin40K dataset, for example, "fine-tuning" the hyperparameters requires an additional 11 minutes and reduces the mean absolute error by an additional 5-8% (depending on the number of random features used to fit).Improving the performance achieved by SVGP, by contrast, would be hard, since if the number of inducing points for SVGP were increased, training time on the larger datasets would become unacceptable.

It is possible that performance for SVGP could be improved by modifying the Adam optimizer settings for stochastic gradient descent, e.g. by dataset-specific tuning of the hyperparameters

of the Adam algorithm, but this is in one sense merely a further drawback for SVGP: xGPR does not require extensive experimentation with optimizer settings to achieve good outcomes. Given these results, we did not implement SVGP for our library, preferring instead the other approximations we will describe shortly.

Table S2. Performance of SVGP (as implemented in the GPyTorch library), random features (as implemented in xGPR) and exact GPs (as implemented in scikit-learn) for various benchmark datasets

Dataset	Split	# training / test datapoints	Metric	GPyTorch SVGP RBF training time (min), 500 inducing points / 3,000 inducing points	GPyTorch score, 500 / 3000 inducing points	xGPR, RBF kernel, training time (min), low / high fitting RFFs	xGPR, RBF kernel, score, low / high fitting RFFs	Exact Gaussian process, RBF kernel, score (if applicable)
Kin40K (UCI)	NA	53,614 / 12,581	MAE (lower is better)	0.5 / 27	0.17 / 0.10	1.5 / 1.8	0.099 / 0.087	
Song (UCI)	Mixed	24,817 / 3,134	MAE (lower is better)	6.4 / 348	0.57 / 0.57	6.0 / 6.9	0.57 / 0.57	
Protein (UCI)	Human only	8,148 / 1,945	MAE (lower is better)	0.5 / 31	0.56 / 0.50	0.69 / 0.78	0.48 / 0.47	
Alpha-adenoviru s (AAV)	Designed vs mutant	201,426 / 82,583	Spearman's r (larger is better)	3.7 / 158	0.58 / 0.63	3.4 / 3.8	0.73 / 0.74	
Alpha adenovirus (AAV)	Mutant vs designed	82,583 / 201,426	Spearmans' r (larger is better)	1.5 / 65	0.67 / 0.65	2.9 / 3.1	0.76 / 0.78	
Alpha adenovirus (AAV)	7 mutations vs many	70,002 / 12,581	Spearmant' s r (larger is better)	1.2 / 54	0.58 / 0.62	1.9 / 2.3	0.67 / 0.68	
Fluorescence	NA	21,446 / 27,217	Spearmant' s r (larger is better)	< 1 / 21	0.66 / 0.67	1.7 / 1.8	0.68 / 0.68	
GB1	3 vs rest	2,968 / 5,765	Spearmant' s r (larger is better)	No data / <1	No data / 0.82	< 1	0.82 / 0.83	0.84
GB1	2 vs rest	427 / 8,306	Spearmant' s r (larger is better)	< 1 / No data	0.48 / No data	< 1	0.62 / 0.62	0.63

S3. Random features

We consider only positive definite kernel functions, and initially only stationary kernels, i.e. kernels for which $K(x_i, x_j) = f(x_i - x_j)$. We seek a transformation $\phi(x)$ such that the kernel $K(x_i, x_j) \approx \phi(x_i)\phi(x_j)$. From Bochner's theorem⁹, any of the positive definite kernels we consider is the Fourier transform of a corresponding positive measure, i.e.:

$$K(x_i, x_j) = \int p(\omega) e^{i \omega^T (x_i - x_j)} d\omega$$

We can approximate this expectation using Monte Carlo sampling, i.e.:

$$K(x_i, x_j) \approx \frac{2}{M} \sum_{k=0}^{M} \cos(\omega_k^T x_i) \cos(\omega_k^T x_j) + \sin(\omega_k^T x_i) \sin(\omega_k^T x_j)$$

Since Monte Carlo approximation is an unbiased estimator of the mean, our estimate converges on the true value as we increase the number of random features. The variance of this estimator is proportional to $(1 / M)^{10}$.

Although this procedure was originally derived in the context of stationary kernels, we can apply a similar Monte Carlo sampling approach to certain nonstationary kernels, most importantly a class of kernels dubbed "neural network kernels" and also called "pointwise nonlinear Gaussian kernels" in more recent literature^{11,12}. Consider a neural network with one hidden layer and one output layer:

$$f(x) = \sum_{i}^{N_{H}} v_{i} h(Wx + b)_{i}$$

where x is an input vector, W is a learned weight matrix of dimensions D x N_H where D is the dimensionality of the input, N_H is the number of units in the hidden layer, b is an offset or bias vector of length N_H , h is some activation function and v_i is a learned weight. Assume that all weights in W are iid drawn from $N(0, \sigma_w^2)$, the weights v_i are iid drawn from $N(0, \sigma_v^2)$ and that the bias terms are iid drawn from $N(0, \sigma_b^2)$. If we augment each x with an additional element that is 1 for all data points, we can rewrite this more simply as:

$$f(x) = \sum_{i}^{N_{H}} v_{i} h(Wx)_{i}$$

Where each row of W is drawn iid from $N(0, \Sigma_W)$, when Σ_W is a diagonal covariance matrix whose first diagonal element is σ_h^2 and all remaining diagonal elements are σ_W^2 .

Let S denote the collection of all weights; it follows that

$$\sum_{S} [f(x_1)f(x_2)] = N_H \sigma_V^2 \sum_{W} [h(Wx_1)_i h(Wx_2)_i]$$

We see that we can once again approximate the expectation term on the right hand side using Monte Carlo sampling and thereby obtain a formulation very similar to the one for stationary kernels. This kernel is only positive definite for certain choices of activation function h^{11} . One such choice is the ReLU activation function which yields the order 1 arccosine kernel¹³, although the error function has also been suggested as a useful activation function¹¹. Interestingly, the order 1 arccosine kernel as formulated in the literature omits the bias terms. During the implementation of our library, we found that the arccosine kernel performs very poorly without the bias term and requires the inclusion of the bias term to achieve acceptable performance.

For both stationary and neural network kernels, then, we can implement the random Fourier features approach as follows. If X is an N x D matrix for N data points and D input features, we populate a D x M matrix with M samples from $p(\omega)$, where $p(\omega)$ is the Fourier transform of the kernel for stationary kernels and the normal distribution for neural network kernels. We multiply this sample matrix by X, and for neural network kernels add an additional bias vector to the result. We then apply the appropriate activation function (e.g. sine and cosine for stationary kernels) and multiply by a constant to yield an N x M matrix Z (or, for stationary kernels, N x 2M). The approximate kernel matrix is then given by ZZ^T .

The distribution across predicted values f_* at new datapoint x_* for a mean-zero Gaussian process given training dataset X with corresponding ground truth values y is:

$$p(f_* | X, y) \sim N(\mu_*, \Sigma_*)$$

$$\mu_* = K(x_*, X)[K(X, X) + \lambda^2 I]^{-1} y, \qquad \sigma_* = K(x_*, x_*) - K(x_*, X)[K(X, X) + \lambda^2 I]^{-1} K(X, x_*)$$

Since we approximate the kernel as ZZ^T , we can use the matrix inversion lemma and the Woodbury matrix identity to rewrite these as:

$$\mu_* = z_*^T [Z^T Z + \lambda^2 I]^{-1} Z^T y, \qquad \sigma_* = \lambda^2 z_*^T [Z^T Z + \lambda^2 I]^{-1} z_*$$

where Z is the training set transformed as described above, I is the identity matrix, λ is a hyperparameter which ensures the kernel matrix is positive definite and z is the new datapoint transformed as described above. If we consider

$$[Z^TZ + \lambda^2 I]^{-1}Z^Ty$$

to be the weights, the predictive mean corresponds to linear regression in the feature space corresponding to the random feature map. It is easy to see the correspondence between a neural network with a single hidden layer plus an output layer and the above kernels approximated using this formulation, although there are several key differences. The approximate GP "learns" by changing the distribution of the hidden layer weights, not individual values, and can be fitted by maximizing the marginal log-likelihood rather than the likelihood; also, the marginal likelihood and the posterior predictive distribution are available in closed form. It is also possible to construct kernels which are analogous to neural networks with several hidden layers. In Supplementary Information section S8 below and under "A new kernel for sequence data" in the main text, we introduce the FastConv-1d kernel, which corresponds to a three-layer neural network with a convolution layer, a fully-connected layer and an output layer, all populated with random weights; this concept is also illustrated in Figure 4 of the main text.

S4. Orthogonal random features

Consider the case where the number of random features D is the same as the dimensionality of the input, d, and where we multiply the input vector x by a matrix M of random features drawn iid from a normal distribution.

If we would like the rows of M to be orthogonal, we can first take the QR decomposition of M, then multiply the resulting Q by a diagonal matrix S whose diagonal elements are drawn from a χ -distribution with d degrees of freedom. The input vector x is now transformed by computing the product kSQx. If the number of random features is greater than d, we can repeat this procedure m times where m is the result of ceiling division of D by d, and then discard any features in excess of D. If D is less than d, we can generate d random features and discard any in excess.

For certain kernels, in particular the squared exponential kernel, it has been shown that fewer orthogonal features are required to accurately approximate the kernel¹², so we achieve a more

accurate approximation for the same number of random features by using orthogonal random features. In addition to this benefit, the orthogonal feature approach can be further modified to realize a large reduction in computational cost. Yu et al.¹⁴ show that we can achieve nearly equivalent results by replacing the matrix Q with the following product:

$$HD_1HD_2HD_3$$

where H is the normalized Hadamard matrix and each D is a separate diagonal matrix whose entries are drawn from the Rademacher distribution. The memory footprint of a fitted model is greatly reduced, because we need to only store the diagonal elements of the D-matrices. More importantly, similar to the substitution of the fast Fourier transform for multiplication with a matrix in the discrete Fourier transform, we substitute the fast Hadamard transform for the Hadamard matrix multiplication, thereby reducing the cost of this procedure to O(D log D) – a dramatic benefit for large M. The general procedure for transforming the input is shown for the RBF kernel in Algorithm S1 (other kernels similar).

Note that Yu et al. 14 suggest replacing the S-matrix used here with multiplication by a constant, \sqrt{d} ; we have found this to fail on 1d data, where the resulting kernel is unable to provide an acceptable fit for simple toy problems, and it provides no benefit on higher dimensional data. Our version from above does not suffer from this limitation.

Algorithm S1 Orthogonal random features transform for RBF kernel

Kernel object initialization

Input: Expected dimensionality d of input; expected number of sampled frequencies M

- 1. $D = 2^{ceiling(log_2(max(d, 2)))}$
- 2. If D < M:
 - a. P = ceiling(M/D)
- 3. Else:
 - a. P = 1
- 4. Create, store diagonal matrix S with size $M \times M$ with elements drawn from the χ -distribution with degrees of freedom D
- 5. For i in 1...P:
 - a. Create, store diagonal matrices $D_{ai'}$ $D_{bi'}$ D_{ci} with size D with elements drawn from the Rademacher distribution

Kernel applied to transform input data

Input: $N \times d$ matrix x_i , which is a chunk of the input data; kernel hyperparameters β , σ **Output:** kernel-transformed matrix Z_i

- 1. For i in 1...P:
 - a. Create empty $N \times D$ array Y_i

- b. Copy x_i into the first d columns of Y_i ; set remaining elements to 0
- c. For k in [a, b, c]:
 - i. $Y_i = H(Y_i D_{ki})$, where H is a normalized in-place fast Hadamard

transform

- 2. Concatenate $Y_1 \dots Y_p$ to form $N \times D^*P$ array Y
- 3. If $D^*P > M$:
 - a. Discard columns M...D*P of Y
- 4. $Y = \sigma YS$
- 5. $Y_1 = cos(Y)$, $Y_2 = sin(Y)$ where sin and cos are applied elementwise
- 6. Concatenate Y_1 and Y_2 to form $N \times 2M$ matrix Z
- 7. $Z = \beta \sqrt{\frac{2}{M}} Z$
- 8. Return Z

S5. Performance of the fast Hadamard transform

We implement a Python-wrapped C / Cuda implementation of the fast Hadamard transform for CPU and GPU. We compare the speed of our implementation with matrix multiplication against a matrix of random features as implemented in the Numpy library (v 1.22.3) and Cupy library for GPU (v 10.4.0) – see Table S2 and S3 for the results. Briefly, our implementation is faster than matrix multiplication for modest numbers of random features, and the performance advantage of our implementation increases with larger numbers of random features as expected, enabling us to quickly scale to large numbers of random features. To compare with other fast transforms, we also compare with the discrete cosine transform (DCT) on CPU as implemented in the Scipy library (v 1.8.0) (Table 1 in the main text).

The results in milliseconds appear in Table S1 and Table S2. In Table S2, we evaluate the time needed to generate random features if the input matrix has as many columns as there are features – this is a somewhat unusual situation but provides a dramatic demonstration of the speed increase for the fast Hadamard transform-based procedure. In Table S3, we consider the more realistic situation where there are a fixed number of 1024 input features and we must generate an increasing number of random features.

We use an input matrix with 2000 rows since this chunk size is common when we work on real datasets. For the GPU implementation, we use 32-bit (single precision) floats due to the substantially greater performance for single precision matrix multiplication on most GPUs, while for the CPU tests we use 64-bit (double precision). In general, however, unless the user selects otherwise, xGPR performs random feature generation using single precision for both CPU and GPU.

Table S3: Speed of the SORF operation implemented in this study (highlighted in the table) compared with vanilla random features and with a generic Scipy fast transform

Algorithm	Average time (ms), 2000 x 2048 input	Average time (ms), 2000 x 4096 input	, ,,,	Average time (ms), 2000 x 16384 input

	matrix	matrix	matrix	matrix
Matrix multiplication, CPU, Numpy, float64	110	450	1700	Not tested (cost prohibitive)
SORF transform, 2 threads, CPU, float64	30	70	160	350
Scipy DCT (3x), float64	80	190	390	880
SORF transform, GPU, float32	6	13	30	60
Matrix multiplication, GPU, Cupy, float32	3.5	13	50	210

The results shown here are rounded to reflect precision, include both CPU time and GPU time (where applicable) and are calculated as the average time per operation for 100 repeats of the specified operation. All experiments were performed on an Intel i5-7500 CPU and a GeForce GTX1070 GPU. The methods used in this study are in bold.

Table S4: Speed of the SORF operation implemented in this study (highlighted in the table) compared with vanilla random features and with a generic Scipy fast transform

Algorithm	Average time for 2048 features (ms), 2000 x 1024 input matrix	Average time for 4096 features (ms), 2000 x 1024 input matrix	Average time for 8192 features (ms), 2000 x 1024 input matrix
Matrix multiplication, CPU, Numpy, float64	56	121.6	236.6
SORF transform, 2 threads, CPU, float64	29.2	58.5	127.6
Scipy DCT (3x), float64	65.5	145.6	286.7
SORF transform, GPU, float32	1.344	2.75	5.1
Matrix multiplication, GPU, Cupy, float32	1.77	3.533	6.56

The results shown here are rounded to reflect precision, include both CPU time and GPU time (where applicable) and are calculated as the average time per operation for 100 repeats of the specified operation. All experiments were performed on an Intel i5-7500 CPU and a GeForce GTX1070 GPU. The methods used in this study are in bold.

S6. Preconditioning for conjugate gradients and stochastic gradient descent

Consider the well-known conjugate gradients algorithm, which solves the system Aw = b for w. It can be shown¹⁵ that the residual error on iteration n has as its upper bound:

$$2\left(\frac{\sqrt{\kappa-1}}{\sqrt{\kappa+1}}\right)^{n}||e_{0}||$$

where κ is the condition number of A, and $||e_0||$ is the error of the initial guess. If κ is large, the algorithm will therefore converge very slowly. A preconditioner whose inverse M^{-1} is a close approximation to the inverse of A will reduce the condition number of A and accelerate convergence¹⁶. It is critical for our purposes to have a preconditioner that can be constructed without explicitly forming the matrix Z^TZ , which will require expensive matrix multiplications and for large numbers of random features will be too large to store in memory.

Kernel matrices for Gaussian processes have frequently been approximated using the Nystrom method, which provides the following low-rank approximation:

$$A \approx A_{m,q} A_q^{-1} A_{m,q}^T$$

where m is the number of rows in A, and q is a randomly selected subset of the columns of A. The Nystrom approximation is cheap to construct and has worked well for many problems in practice¹⁷. Although sampling from a uniform distribution has traditionally been the most popular approach, the performance of this method is sensitive to the sampling method used to select columns and rows in A¹⁸.

We found the randomized Nystrom approximation described by Alaoui et al.¹⁹ to provide better performance. In this scheme, for the system:

$$(Z^TZ + \lambda^2 I)^{-1}Z^Ty = w$$

A low-rank approximation of $Z^TZ = A$ is provided by:

$$A_{nystrom} \approx (A\Omega)(\Omega^T A\Omega)^{\dagger}(A\Omega)^T$$

where for Ω we use an iid matrix drawn from a zero mean, unit-variance normal distribution; Ω is of size M x L, where M is the number of random features. This approach provides a rank-L approximation to A, and a numerically stable approach for generating it (which we implement for our library) is described in Martinsson et al.²⁰ and appears in Algorithm S2. Importantly for our purposes, we can construct this as shown *without* ever explicitly forming the matrix Z^TZ and using a single loop over the dataset, loading one chunk of the data into memory at a time.

Algorithm S2 Constructing a randomized Nystrom preconditioner

Input: Dataset X stored in chunks $x_1 \dots x_n$ on disk, desired preconditioner size L, GP kernel, number of random features M

Output: Factored preconditioner in the form $U\Lambda U^T$, where U is orthonormal and Λ is diagonal

- 6. Generate $M \times L$ matrix Ω by sampling from N(0, 1)
- 7. $\Omega = gr(\Omega)$

QR decomposition

- 8. Generate M x L matrix Q and initialize to all zeros
- 9. For i in 1...n, load x_i
 - a. Use Algorithm S1 to generate z_i

b.
$$Q += z_i^T(z_i\Omega)$$

10.
$$v = \sqrt{M}eps(norm(Q))$$

11. $Q_{\nu} = Q + \nu \Omega$	For numerical stability
12. $C = cholesky(\Omega^T Q_{v})$	
13. $CB = Q_{v}$	Triangular solve for B
14. U , Σ , $\sim = svd(B)$	SVD of B
15. $\Lambda = max(0, \Sigma^2 - \nu I)$	
16. Return <i>U</i> , Λ	

We here introduce a novel modification. We replace the M x L matrix Ω with the subsampled randomized Hadamard transform, which is defined as follows:

$$SRHT = \sqrt{\frac{M}{L}}SHD$$

Where *D* is a diagonal matrix with entries drawn from the Rademacher distribution, H is the normalized Hadamard matrix, and S is a subset of L rows drawn with equal probability from the identity matrix. In practice, of course, we use the fast Hadamard transform rather than the Hadamard matrix. For step 9b, we then substitute:

$$Q += SRHT(Z^T)Z$$

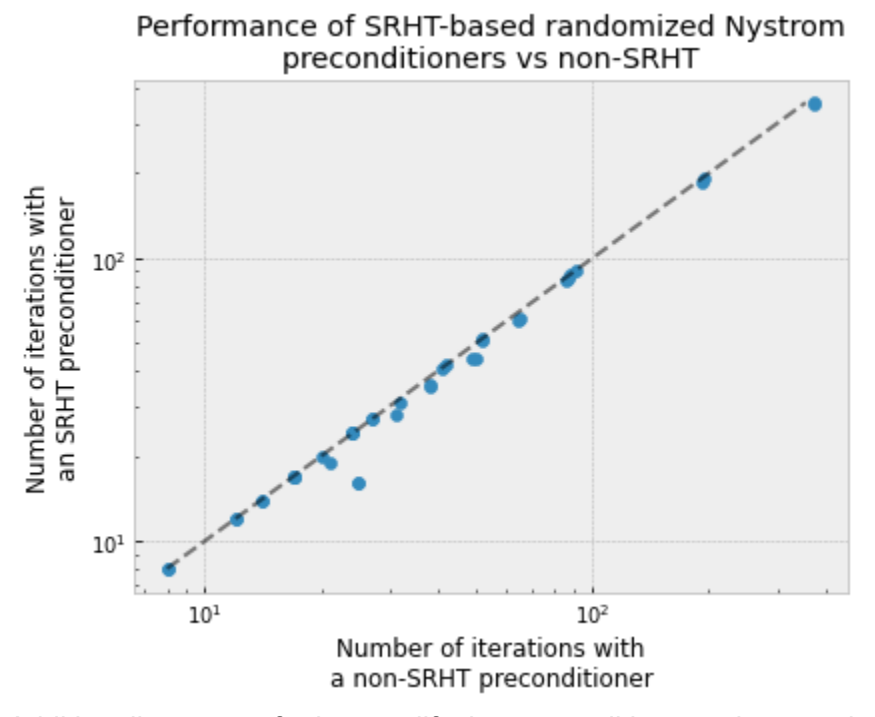
In step 12, for the product $\Omega^T Q_{_{V}}$, we substitute $SRHT(Q_{_{U}})$. Finally, to ensure numerical stability, we replace the shift-then-subtract procedure above (steps 11 and 15) with a procedure outlined by Li et al.²¹, wherein rather than taking the Cholesky decomposition of $SRHT(Q_{_{U}})$ in step 12, we find the self-adjoint square root of this matrix using SVD, then use this to solve for B in the following step.

Using the SRHT to construct low-rank matrix approximations has been suggested before (see Halko et al. 22 and Boutsidis et al. 23 for example), but not to construct a preconditioner for CG / stochastic gradient descent as we suggest here (at least not to our knowledge). It significantly reduces the cost of preconditioner construction, since we replace a matrix multiplication with O(NML) scaling with a fast transform operation; this is especially advantageous if working on CPU. Empirically, we have found the SRHT-based preconditioner construction routine to be substantially faster even for datasets of only 40,000 datapoints, and the advantage increases with increasing dataset size and number of random features.

In every case we encountered, we found empirically that a preconditioner constructed using SRHT as we suggest here performed either as well as or *better than* a preconditioner constructed using the unmodified algorithm S2. In Figure S1 below, we compare the number of iterations required for conjugate gradients to converge to a pre-specified threshold using a preconditioner constructed either with SRHT or with the unmodified algorithm S2, using a variety of different values for *L*. We see that in every case, the SRHT-built preconditioner

achieves the same or greater acceleration, and indeed this has been consistently true throughout our experiments. For the time being, we provide both the modified and unmodified preconditioner construction algorithms as options the user can select in xGPR and default to the SRHT-based algorithm in light of its superior speed and empirical performance. A theoretical analysis of the merits of each approach is beyond the scope of this paper, given the many other problems we are already tackling; we defer such an analysis to future work.

Figure S1. A comparison of the acceleration achieved for conjugate gradients using a preconditioner constructed using SRHT or using the unmodified Algorithm S2.

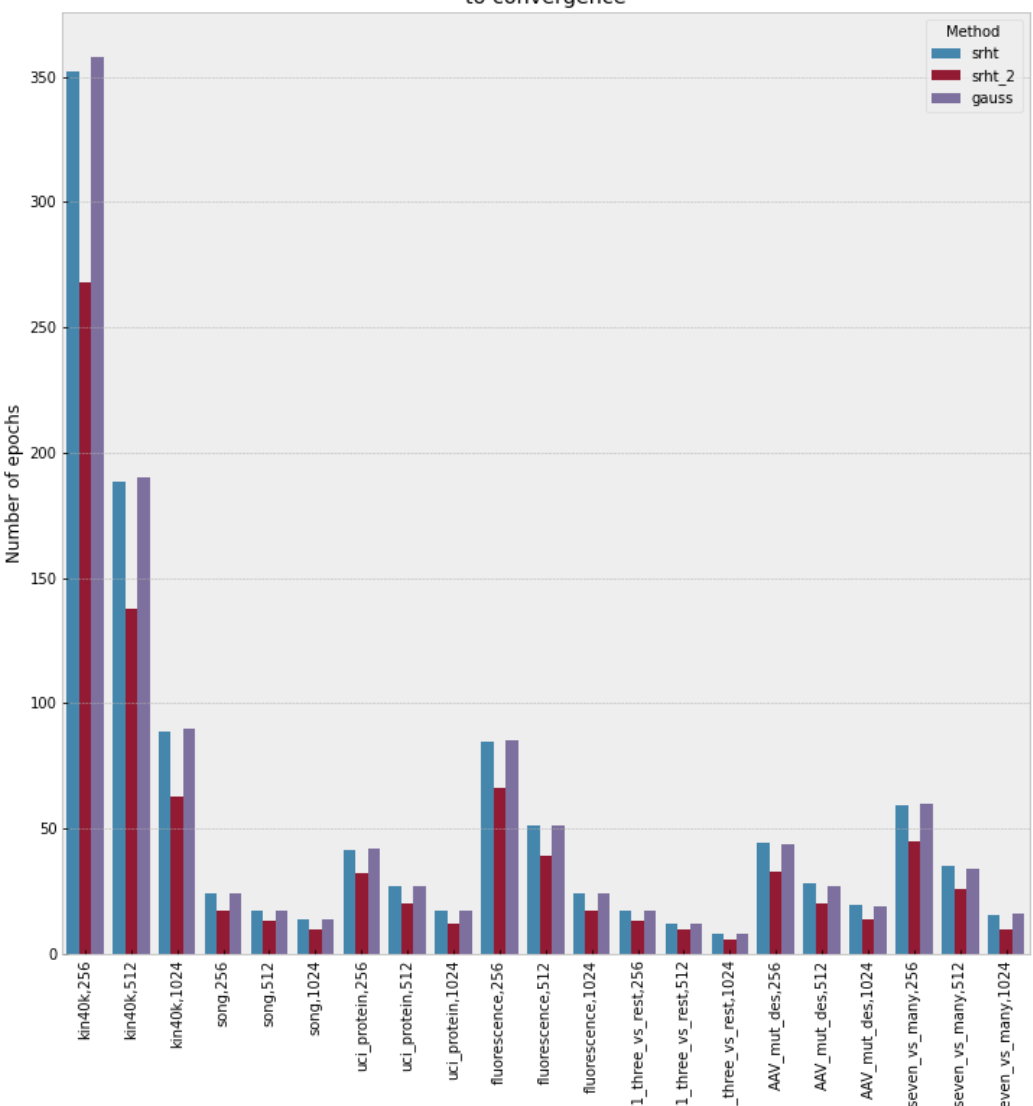


Additionally, we can further modify the preconditioner to improve its performance. In step 9 of Algorithm S2, we form the product $Z^T(Z\Omega)$, where Z is the matrix of random features for the training data of shape N x M for M random features and N datapoints. We can retrieve the matrix Q from the QR decomposition of this product and use this to form a second product

 $Z^T(ZQ)$ using a second pass over the dataset. We then use this product in Algorithm S2 in place of the matrix Q from step 9. (We can even repeat this process a third time, although this offers a negligible improvement in preconditioner performance.) As expected, the resulting preconditioner reduces the number of iterations required for conjugate gradients to converge in all of our experiments, in most cases by 20-25%, as illustrated in Figure S2 below. It is however more expensive to construct since it requires two passes over the dataset. Whether this is beneficial will depend on the size of the dataset and on available hardware. We therefore allow the user to select "srht_2" as an option for preconditioner construction in xGPR and provide guidance in the documentation on when to choose this option.

Figure S2. The number of iterations to convergence across various benchmark datasets using various settings for preconditioner rank and three different variants on the preconditioner construction algorithm.

Preconditioner construction algorithm vs preconditioner rank & number of epochs to convergence



Irrespective of which option is used to construct it, the inverse of the preconditioning matrix takes the form:

$$M^{-1} = (\beta_L + \lambda^2)U(\Lambda + \lambda^2 I)^{-1}U^T + (I - UU^T)$$

Where β_L is the smallest eigenvalue of the preconditioner and λ is a hyperparameter of the GP kernel. We do not of course actually form the matrix \boldsymbol{M}^{-1} explicitly, but since we have generated all the needed values above, we can supply the matrix-vector product \boldsymbol{M}^{-1} \boldsymbol{v} on demand, which is all that is required for preconditioned conjugate gradients or preconditioned stochastic gradient descent.

The larger L, the better the approximation; if $\beta_1 \geq \beta_2 \geq \beta_3$... are the eigenvalues of A, the approximation is also better the more rapidly the eigenvalues decay, and the smaller the eigenvalues for $\beta_{j\geq L}$. Let $U\Lambda U^T$ be the eigendecomposition of $A_{nystrom}$ of rank L, let the preconditioner P be $P = \frac{1}{\beta_L + \lambda^2} U(\Lambda + \lambda^2 I) U^T + (I - UU^T)$, and let β_L be the smallest eigenvalue of $A_{nystrom}$. It can be shown²⁴ that if κ_2 is the condition number of the preconditioned system, the probability that:

$$max(0, \kappa_2(P^{1/2}(\lambda^2 I + Z^T Z) P^{1/2}) - \frac{\beta_L + \lambda^2}{\lambda^2}) \le \frac{\beta}{\delta}$$

will be $\geq 1 - \delta$, where δ is some failure tolerance.

How to choose L? The value of $\frac{\beta_L}{\lambda^2}$ for a given L can be estimated by constructing a preconditioner, and the value of L can then be doubled until $\frac{\beta_L}{\lambda^2}$ suggests the number of iterations required to fit the model is likely to be acceptable. As illustrated in Figure 1a from the main text, the log of the number of iterations often exhibits a roughly linear relationship with $\frac{\beta_L}{\lambda^2}$ for a given desired tolerance. Consequently, we can estimate the number of iterations required to fit for a given $\frac{\beta_L}{\lambda^2}$ and if we consider the resulting number of iterations to be too high, we can adjust L and reconstruct the preconditioner. For more explicit guidance on how to choose a preconditioner, refer to the xGPR documentation at https://xgpr.readthedocs.io/en/latest/.

S7. Improved strategies for optimization

Recall that for a Gaussian process we find the following for the negative marginal log likelihood:

$$-log \ p(y \mid X) \ = - \ log \ \int p(y \mid f, \ X) \ p(f \mid X) \ df \ = \ \frac{1}{2} y^T K_y^{-1} y \ + \frac{1}{2} log |K_y| \ + \ \frac{N}{2} log (2\pi)$$

Where $K_y = K(X, X) + \lambda^2 I$. In the random features scheme, we substitute our approximation $Z^T Z$ for K(X, X) and rearrange to yield:

$$-\log p(y \mid X) = \frac{-1}{2\lambda^2} y^T Z (Z^T Z + \lambda^2 I)^{-1} Z^T y + \frac{1}{2\lambda^2} y^T y + (n-m) \log(\lambda) + \frac{1}{2} \log|Z^T Z + \lambda^2 I| + \frac{n}{2} \log(2\pi)$$

 Z^TZ is Hermitian so that as long as it is full-rank, we can generate an eigendecomposition $P\Lambda P^T$ such that P is orthonormal, i.e. $PP^T = I$. We then rearrange the above expression:

$$-\log p(y \mid X) = \frac{-1}{2\lambda^2} y^T Z P \left(\Lambda + \lambda^2 I\right)^{-1} P^T Z^T y + \frac{1}{2\lambda^2} y^T y + (n-m) \log(\lambda) + \frac{1}{2} \log|\Lambda + \lambda^2 I| + \frac{n}{2} \log(2\pi)$$

For three and four hyperparameter kernels, we can make use of this simplification in a variety of ways, for example Algorithm S3 and Algorithm S4.

Algorithm S3 Efficient grid search

Input: Dataset X with N datapoints stored in chunks $x_1 \dots x_n$ and $y_1 \dots y_n$ on disk, initialized kernel with two, three or four hyperparameters (λ , β , σ_1 , if applicable σ_2) for M random features, selected values for hyperparameters (if applicable) σ_1 and σ_2

- 1. Initialize M x M array W and M x 1 array S, set to zero
- 2. a = 0
- 3. For j in 1...N:
 - a. Load x_{j} , y_{j} and use Algorithm S1 to form $Q_{j} = Z_{j} / \beta$ using δ_{i}
 - b. $W += Q^T Q$; $S += Q^T y$
 - c. $a += y_i^T y_i$
- 4. U, $\Lambda = eigh(W + \delta I)$ add small constant delta for numerical stability
- 5. $\Lambda -= \delta$
- 6. $S = U^T S$
- 7. Define loss_ $fn(\beta, \lambda)$:
 - a. Return $\frac{-1}{2\lambda^2}S(\Lambda + \lambda^2 I)^{-1}S + \frac{1}{2\lambda^2}y^Ty + (n-m)log(\lambda) + \frac{1}{2}log(\Lambda + \lambda^2 I) + \frac{n}{2}log(2\pi)$
- 8. λ_{best} , $\beta_{best} = argmin_{\lambda,\beta}loss$
- 9. $Score = loss(\lambda_{best}, \beta_{best})$

Return *Score*, λ_{best} , β_{best}

Algorithm S4 Bayesian hyperparameter optimization (Thompson sampling)

Input: Dataset X with N datapoints stored in chunks $x_1 \dots x_n$ and $y_1 \dots y_n$ on disk, initialized kernel with three or four hyperparameters (λ , β , σ_1 , if applicable σ_2) for M random features, maxiter maximum iterations, n candidates per iteration, convergence criteria tol

- 1. Evaluate score, λ_{best} , β_{best} for 5 10 randomly selected kernel-specific hyperparameters ω_1 ... ω_{10} using Algorithm S3
- 2. Let Ω be the set of all kernel-specific hyperparameter combinations evaluated thus far; let ω_{hast} be the best evaluated so far
- 3. For niter in 10...maxiter:
 - a. Fit exact Gaussian process S with Matern kernel, v = 5/2
 - b. Draw n kernel-specific hyperparameter combinations ω_1 ... ω_n from $Uniform(\sigma_{max}, \sigma_{min})$
 - c. Draw *m* samples from *S* at each of $\omega_1 \dots \omega_n$; select $\omega_{new} = argmin_{\omega}(m)$
 - d. If $||\omega_{new} \omega_{best}||_2 < tol$:
 - break
 - e. Evaluate the loss function from Algorithm S3 at $\omega_{\it new}$
 - $\begin{array}{ll} \text{f.} & \text{If } loss_{new} < \ loss_{best} \text{:} \\ & \text{i.} & \omega_{new} \ = \ \omega_{best} \end{array}$
- 4. Return ω_{best}

Note that we use Thompson sampling in S4, but of course other acquisition functions (e.g. expected improvement) can easily be substituted as well. We can also use a simple grid search across the kernel-specific hyperparameter, which is also implemented in xGPR. We can also modify the above algorithm by calculating the eigendecomposition of Z^TZ by taking the singular value decomposition of Z, which is of course the most stable approach.

The polynomial kernel has only two hyperparameters (the lambda or noise and beta or amplitude hyperparameters shared with all other kernels). Using the strategy above, these can be tuned using a *single pass over the data*, so that hyperparameter tuning with the polynomial kernel is exceptionally fast.

Clearly, however, this strategy scales poorly to large datasets and large numbers of random features, and is therefore mostly useful as a means to generate a starting point for further optimization. (Surprisingly, we often find this starting point provides performance good enough

that no further optimization is required!) We therefore develop an approach for estimating marginal likelihood for large numbers of random features.

S8. Log determinant approximation and conjugate gradients

A variety of approaches have been outlined in the literature for approximating the log determinant of a large matrix A, including stochastic Lanczos quadrature²⁵, stochastic trace estimation combined with Chebyshev polynomials²⁶, and subspace iteration²⁷. The subspace iteration method of Saibaba et al. is only appropriate if a small subset of the eigenvalues of A are dominant, i.e. there is a large eigengap with eigenvalue $\lambda_i >> \lambda_{i+1}$, $\lambda_{i+2} \dots \lambda_N$, which is not always true during tuning.

Stochastic Lanczos quadrature (SLQ) is especially attractive in this context, since for large numbers of random features we use preconditioned conjugate gradients to fit the model, and we can automatically generate the tridiagonal matrices required for stochastic Lanczos quadrature during the course of the conjugate gradients optimization at negligible additional cost (see Saad 2003¹⁵). Gardner et al.²⁸ have already demonstrated the use of this approach to accurately estimate log determinants for exact (non-approximated) Gaussian processes using an incomplete Cholesky decomposition to build the preconditioner.

In Algorithm S5 below, we show how to use this approach in combination with the random features approximation and the randomized Nystrom approximation to accurately estimate the log determinant term, $\frac{1}{2}log|Z^TZ + \lambda^2I|$, while simultaneously calculating the performance penalty $\frac{-1}{2\lambda^2}y^TZ(Z^TZ + \lambda^2I)^{-1}Z^Ty$ (the remaining terms in the marginal likelihood are either constants or do not require us to retrieve the data and hence are easily calculated). The resulting algorithm exhibits linear scaling with dataset size, subquadratic scaling with number of random features, and never requires us to load more than one chunk of data into memory at a time.

As a preliminary, we first rewrite the log determinant and make use of Hutchison's trace estimator²⁹:

$$log|Z^TZ + \lambda^2 I| = trace(log(Z^TZ + \lambda^2 I)) \approx \frac{1}{n_v} \sum_{i=1}^{n_v} p_i^T log(Z^TZ + \lambda^2 I) p_i$$

Where p_i are probe vectors drawn(typically) from either a Rademacher or a Gaussian distribution.

Next, we note that when we use preconditioned conjugate gradients with preconditioner P, we are in fact solving the preconditioned system $log | P^{-1/2} Z^T Z + \lambda^2 I P^{-1/2} |$. We can adopt the same approach that Gardner et al.²⁸ adopt for exact (un-approximated) GPs and rewrite this as:

$$log|Z^{T}Z + \lambda^{2}I| = log|P^{-1/2}(Z^{T}Z + \lambda^{2}I)P^{-1/2}| + log|P|$$

$$log|P^{-1/2}(Z^{T}Z + \lambda^{2}I)P^{-1/2}| = trace(P^{-1/2}log(Z^{T}Z + \lambda^{2}I)P^{-1/2}) \approx \frac{1}{n_{v}} \sum_{i=1}^{n_{v}} p_{i}^{T}P^{-1/2}log(Z^{T}Z + \lambda^{2}I)P^{-1/2}p_{i}$$

We therefore need to apply the preconditioner to the probe vectors. This is easily done if the probe vectors are drawn from a Gaussian; we can merely draw them from a normal distribution whose covariance matrix is our preconditioner. We now refer to these preconditioned probe vectors as \boldsymbol{c}_i .

We now need to evaluate the term

$$\frac{1}{n_{v}} \sum_{i=1}^{n_{v}} c_{i}^{T} P^{-1/2} log(Z^{T}Z + \lambda^{2}I) P^{-1/2} c_{i}$$

We do so using the quadrature-based procedure of Ubaru et al. 25 , but using the preconditioned conjugate gradients algorithm; by storing the alpha and beta coefficients produced on each iteration of conjugate gradients, we generate the same tridiagonal matrix that Ubaru et al. construct via the Lanczos algorithm. We merely need in this case to run conjugate gradients with multiple target vectors – both the Z^Ty vector so that we can calculate the performance penalty $(Z^TZ + \lambda^2I)^{-1}Z^Ty$, and the preconditioned probe vectors so that we can generate n_v tridiagonal matrices $T_1, T_2 \dots T_{n_v}$. A simplified version of the full procedure is outlined in Algorithm S5 below.

Algorithm S5 Preconditioned conjugate gradients for simultaneous estimation of $(Z^TZ + \lambda^2 I)^{-1}Z^Ty$ and $log|Z^TZ + \lambda^2 I|$

Input: Dataset X with N datapoints stored in chunks $x_1 \dots x_n$ and $y_1 \dots y_n$ on disk, initialized kernel with fixed hyperparameters that generates length-M random feature representation $k(x_i)$ for input datapoint x_i , preconditioner P constructed using Algorithm S2 or appropriate variant, number of probe vectors n_i , convergence threshold tol

- 1. Create empty array $Z^{T}y$ of shape M
- 2. For i in 1,2...*n*:

a.
$$Z^T y += k(x_i)^T y_i$$

- 3. For i in 1,2... n_v :
 - a. Draw probe vector c_i from N(0, P)
- 4. Create empty array $r_{_{j}}$ of shape (M, $n_{_{\boldsymbol{v}}}$ +1)
- 5. Populate the first n_v columns of r_j with c_1 , c_2 , c_3 ... c_{n_v} . Copy Z^Ty into the remaining column.
- 6. Let $L_1=[||r_{j1}||,\ ||r_{j2}||,\ ||r_{j3}||....\ ||r_{jn_v+1}||]$ where $||r_{jk}||$ is the Euclidean norm of column k in r_j , such that L_1 is a row vector of length n_v+1
- 7. Create initial weight matrix w_i of shape (M, $n_v + 1$); set all entries to zero.
- 8. Create empty array B of shape (M, n_v+1). Let 1_M be a length-M vector of ones. Let err be a length n_v+1 vector of ones.

9.
$$p_j = z_j = P^{-1}r_j$$
; $j = 1$

- 10. While max(err) > tol and j < maxiter:
 - a. Set all entries of B to zero
 - b. For i in range 1,2...*n*:

i.
$$B += k(x_i) k(x_i)^T p_k$$

c.
$$B += \lambda^2 p_i$$

d. $\alpha_j = \frac{1_M^T(r \circ z_j)}{1_M^T(p_j \circ B)}$ with elementwise division, such that α_j is a row vector of length n_v +1

e.
$$w_j += (1_M \alpha_j) \circ p_j$$

f.
$$r_{i+1} = r_i - (1_M \alpha_i) * B$$

- g. Let $err = [||r_{j1}||, \ ||r_{j2}||, \ ||r_{j3}||.... \ ||r_{jn_v+1}||]$ where $||r_{jk}||$ is the Euclidean norm of column k in r_j , such that err is a row vector of length n_v+1 where $||r_{ji}||$ is the norm of column i in r_j
- h. $err = err / L_{_1}$ with elementwise division

i.
$$z_{j+1} = P^{-1}r_j$$

j. $\beta_j = \frac{1_M^{T}(r_{j+1} \circ z_{j+1})}{1_M^{T}(r_j \circ z_j)}$ with elementwise division, such that β_j is a row vector of length $n_j + 1$

k.
$$p_{j+1} = z_{j+1} + (1_M \beta_j) \circ p_j$$

I. Store
$$\beta_j$$
, α_j

m.
$$j += 1$$

- 11. Let α_{ik} be the element of α_k corresponding to iteration k and probe vector i (corresponding to column i+1 of p_j). Let β_{ik} be the element of β_k corresponding to iteration k and probe vector i (corresponding to column i+1 of p_j).\
- 12. $\Gamma = 0$
- 13. For i in 1,2... n_v :
 - a. Create empty matrix T of shape (j, j). Set all entries to zero.
 - b. For k in 1,2...*j*:

i.
$$T_{kk} = \frac{1}{\alpha_{ik}}$$

c. For k in 1,2...*j-1*:

i.
$$T_{k+1,k+1} += \frac{\beta_{ik}}{\alpha_{ik}}$$

ii.
$$T_{k,k+1} = T_{k+1,k} = \frac{\sqrt{\beta_{ik}}}{\alpha_{ik}}$$

d.
$$[Y, \Theta] = Eig(T);$$
 $\tau_m = e_1^T y_m$ for m in $1, 2... j$

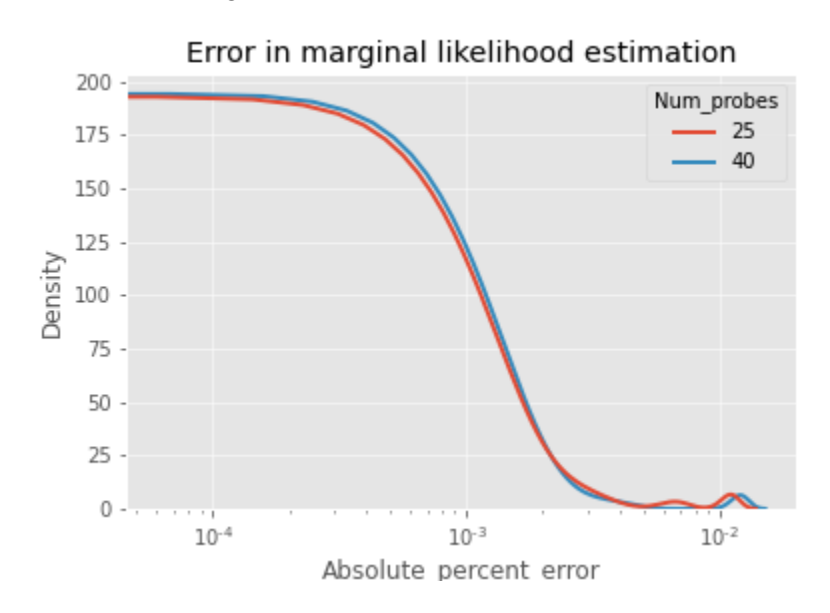
e.
$$\Gamma += \sum_{m}^{j} \tau_{m} log(\theta_{m})$$

14.
$$\Gamma = \Gamma * \frac{M}{n_v}$$

15. Return estimated log determinant Γ , vector $Z^T y$ and column 1 of w_j ; this last corresponds to $(Z^T Z + \lambda^2 I)^{-1} Z^T y$ and can be used to calculate the performance term of the negative marginal log likelihood

To evaluate the accuracy of this procedure, we randomly select 8 hyperparameter combinations each for 7 different datasets ranging in size from a few hundred datapoints to half a million. For each, we calculate the negative marginal log likelihood with 4,096 random features either using Algorithm S5 or using matrix decompositions, using a preconditioner rank of 512, a convergence threshold of 1e-5 and the "srht_2" preconditioner construction algorithm in all cases. We use either 40 probe vectors or 25 probe vectors; the distribution of the absolute percent error is plotted in Figure S3 below. 40 probe vectors does not provide a substantial improvement on 25 probe vectors. Remarkably, 25 probe vectors is sufficient in this experiment to achieve high accuracy.

Figure S3. Distribution of absolute percent error for marginal likelihood estimation across 112 evaluations using either 25 or 40 probe vectors.



To further assess the accuracy of this procedure, we use approximate marginal likelihood in combination with Bayesian optimization to tune hyperparameters for two of the tutorials / example experiments in the user documentation (available at https://xgpr.readthedocs.io/en/latest/). The first such experiment involves the UCI proteins dataset, the second involves the QM9 dataset with one-hot encoded inputs. In both cases, the tuning procedure improves on the best validation set performance achieved by tuning with a smaller number of random features with a matrix decomposition-based approach. We further use the same approach to tune hyperparameters for the tabular data and the small molecule experiments on the QM9 dataset described in the main text and are able as described in the main text to achieve highly competitive performance. These results are consistent with the experiment from Figure S3 above and suggest that given an adequate preconditioner rank, a sufficiently small convergence threshold, and a sufficient number of probe vectors, for the datasets we consider here, Algorithm S5 is able to estimate the negative marginal log likelihood with high accuracy.

<u>Lemma 1.1.</u> Let $K: \mathbb{R}^D x \mathbb{R}^D \to \mathbb{R}$ be a positive definite kernel on \mathbb{R}^D , and let $f: X \to \mathbb{R}^D$ be any mapping from X to \mathbb{R}^D , where X is some non-empty set. Then K(f(u), f(w)) is a positive definite kernel on X for $u, w \in X$.

<u>Proof</u>: Let $f: X \to \mathbb{R}^D$ be any mapping from X to \mathbb{R}^D , where X is a non-empty set. Let $K: \mathbb{R}^D x \mathbb{R}^D \to \mathbb{R}$ be a positive definite kernel on \mathbb{R}^D , i.e.:

$$\sum_{i}^{N} \sum_{j} c_{i} c_{j} K(x_{i}, x_{j}) \ge 0$$
 (1.1a)

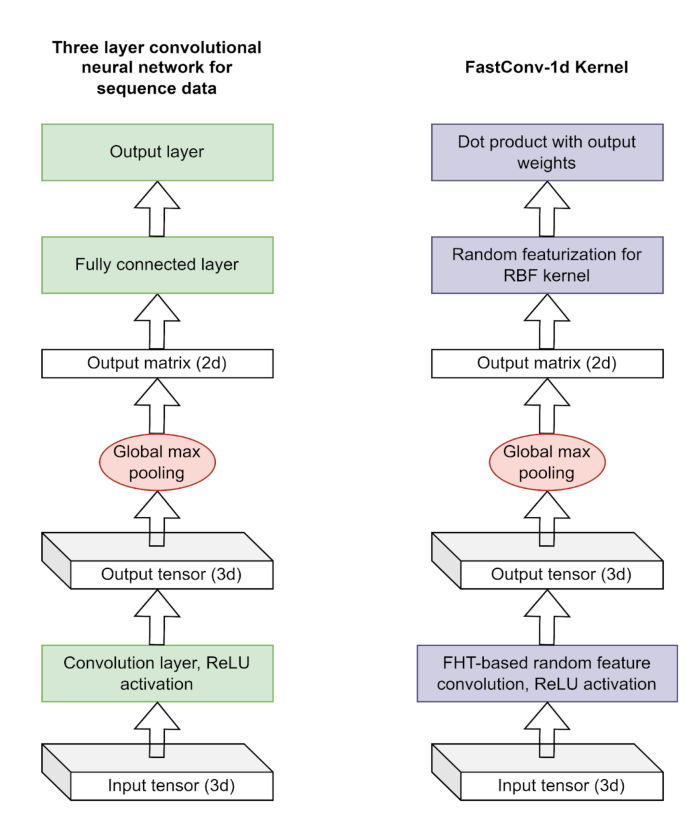
for any choice of $x_1, x_2, x_3 \dots x_n \in \mathbb{R}^D$ and for any choice of $c_1, c_2, c_3 \dots c_n \in \mathbb{R}$. Since this is true for any arbitrary selection of $x_1, x_2, x_3 \dots x_n \in \mathbb{R}^D$, and since f maps its input into \mathbb{R}^D , it is also true that

$$\sum_{i}^{N} \sum_{j} c_{i} c_{j} K(f(x_{i}), f(x_{j})) \geq 0$$

for any choice of $x_1, x_2, x_3 \dots x_n \in X$.

In other words – this is merely another way to say that any feature engineering process or function which constructs a representation in \mathbb{R}^D can be "plugged into" a kernel which is positive-definite on \mathbb{R}^D and retain the positive definite property. We can use this to construct "plug-in" kernels, e.g. the FastConv1d kernel in the text.

Figure S4 Comparison of a three-layer convolutional neural network for sequence data with a FastConv-1d kernel. Note the similar structure combined with some key differences (e.g. the convolution in FastConv-1d is random feature-based and can be performed offline, the kernel is used in a GP which is a Bayesian model whereas the convolutional network is trained to maximize the marginal likelihood, etc.)



S10. Polynomial kernels on graphs

A kernel sometimes used for small molecules is the SOAP kernel of Bartok et al.³⁰ This kernel constructs a fixed-length vector description of each atom by expanding the "smeared" density of an atom and its neighbors into a truncated orthonormal basis set. The more basis functions used, the more accurate the description and the longer the descriptor vector. A polynomial kernel is then evaluated pairwise across all atoms in two molecules using these features as input. The SOAP kernel for two molecules is then evaluated as follows:

$$\sum_{i}^{N_{1}N_{2}} \sum_{j} \left(\frac{p_{i}^{T} p_{j}}{\sqrt{p_{i}^{T} p_{i}^{T} p_{i}^{T}}} \right)^{\zeta}$$

Where p is a SOAP descriptor vector and the sum is over all atoms in the two molecules. Notice that if the descriptor vectors are normalized to be unit-norm, this is essentially just a polynomial kernel, $k(x_1, x_2) = (x_1^T x_2)^\zeta$ evaluated over all pairs of atoms in two molecules. This approach has $O(D^2)$ scaling with graph size. We now introduce a novel highly efficient way to use polynomial kernels on graphs, which we refer to as the GraphPoly kernel.

We can approximate a polynomial kernel via random features – see for example Wacker et al.³¹. If we approximate a polynomial kernel using random features such that $k(x_1, x_2) \approx z_1^T z_2$, we can approximate the SOAP kernel (or any other polynomial kernel evaluated pairwise over all

vertices in two graphs) as $(\sum\limits_{i}^{N_{1}}z_{i})^{T}(\sum\limits_{j}^{N_{2}}z_{j})$. This approach scales linearly with the number of datapoints and the size of the graph, which is a huge reduction in cost. We implement this as the GraphPoly kernel in xGPR.

This kernel is clearly less flexible than the graph convolution kernel described in the main text, since it is only applicable if a polynomial kernel is an appropriate measurement of the similarity of two vertices (or two atoms) in the two graphs. However it may be more useful for certain niche tasks, especially prediction of energetic and thermodynamic properties of small molecules, where the SOAP kernel has already demonstrated impressive results³².

S11. Comparison of FHTConv1d with FastConv1d, and of Gaussian process approximations using one-hot encoded input with pretrained protein language models. In the main text, we compare the best performer from the FHTConv1d and FastConv1d kernels with the deep learning model. The performance of FHTConv1d and FastConv1d is also compared in Figure 4 of the main text. We here in Table S3 provide a more detailed comparison of the FHTConv1d and FastConv1d kernels with the CNN baselines from Dallago et al. and Rao et al. As noted in the main text, FastConv1d and FHTConv1d achieve similar performance on these benchmarks. We omit multiple sequence alignment (MSA) data, for which we use an RBF kernel since these sequences are already of the same length. We also omit the Thermostability dataset, for which we only used the FastConv1d kernel; due to the long length of these sequences, the FastConv1d kernel is much faster.

Table S5. A more detailed comparison of kernels on protein sequence benchmark datasets

Dataset	Split ^a	Data type	# training / test datapoints	Deep learning architecture	Spearman's-r for deep learning model trained on one-hot data	Source	Spearman's R for FHTConv1d using 8,192 / 16,384 RFFs	Spearman's R for FastConv1d using 8,192 / 16,384 RFFs
Stability	Stability	Zero-padded, unaligned	53,614 / 12,581	Convolutional neural net	0.51	Dallago et al	0.608 / 0.660	0.619 / 0.611
Thermostability	Mixed	Zero-padded, unaligned	24,817 / 3,134	Convolutional neural net	0.34	Dallago et al		0.352 / 0.366
Thermostability	Human only	Zero-padded, unaligned	8,148 / 1,945	Convolutional neural net	0.5	Dallago et al		0.553 / 0.564
Alpha adenovirus (AAV)	Designed vs mutant		201,426 / 82,583	Convolutional neural net	0.75	Dallago et al	0.764 / 0.775	0.761 / 0.776
Alpha adenovirus (AAV)	Mutant vs designed	Zero-padded, unaligned	82,583 / 201,426	Convolutional neural net	0.71	Dallago et al	0.734 / 0.750	0.747 / 0.757
Alpha adenovirus (AAV)	7 mutations vs many	Zero-padded, unaligned	70,002 / 12,581	Convolutional neural net	0.74	Dallago et al	0.712 / 0.724	0.686 / 0.700
Alpha adenovirus (AAV)	2 mutations vs many	Zero-padded, unaligned	31,807 / 50,776	Convolutional neural net	0.74	Dallago et al	0.570 / 0.590	0.658 / 0.674
Alpha adenovirus (AAV)	1 mutation vs many	Zero-padded, unaligned	1,170 / 81,413	Convolutional neural net	0.48	Dallago et al	0.574 / 0.560	0.781 / 0.792

In Table S5, we next reproduce some results from Dallago et al. and Rao et al. involving pretrained models applied to the protein engineering benchmarks discussed in the main body of the paper. We omit the results from Dallago et al.⁴ for "untrained weights". These results can be compared with those in Table 3 of the main paper and Table S4 above. It becomes immediately apparent that the performance of the pretrained models and representations derived from them depends heavily on how those representations are used, and even then, there is no clear or consistent trend in terms of which pretrained models perform best. Again, for the thermostability dataset we only used the FastConv1d kernel; due to the long length of these sequences, the FastConv1d kernel is much faster. The FHTConv1d kernel can be used for these datasets also but is much slower because of the long length of the sequences.

Table S6. Performance (Spearman's-r) of pretrained language models on protein

engineering benchmarks from Dallago et al.

<u> </u>						
Dataset	Split	# training / test datapoints	Score for ESM-1b, per AA	Score for ESM-1v, per AA	Score for ESM-1b, mut mean pooling	Score for ESM-1v, mut mean pooling
Alpha-adenovirus (AAV)	Designed vs mutant	201,426 / 82,583	ND	ND¹	0.7	0.71
Alpha adenovirus (AAV)	Mutant vs designed	82,583 / 201,426	0.76	0.79	0.7	0.7
Alpha adenovirus (AAV)	7 mutations vs many	70,002 / 12,581	0.65	0.7	0.61	0.64
Alpha adenovirus (AAV)	2 mutations vs many	31,807 / 50,776	0.65	0.7	0.65	0.64
Alpha adenovirus (AAV)	1 mutation vs many	1,170 / 81,413	0.03	0.1	0.31	0.44
GB1	3 vs rest	2,968 / 5,765	0.79	0.82	0.49	0.8
GB1	2 vs rest	427 / 8,306	0.55	0.28	0.19	0.19
Thermostability	Mixed	24,817 / 3,134	0.68	0.65	_2	_
Thermostability	Human only	8,148 / 1,945	0.71	0.77	-	-

¹ No data; ² Not tested

Table S7. Performance (Spearman's-r) of pretrained language models on protein engineering benchmarks from Rao et al.

Dataset	Split	# training / test datapoints	Score for Protein BERT	Score for Unirep, Rao et al	Score for "Bepler" embedding, Rao et al
Fluorescence	NA	21,446 / 27,217	0.68	0.67	0.33
Stability	NA	53,614 / 12,581	0.73	0.73	0.64

In principle, the pretrained models should always outperform a CNN or a GP trained solely on one-hot encoded input, since they have access to a large corpus of training information not available to the CNN or GP. The only case where the pretrained models seem to behave as expected however is the stability datasets. In this instance, given the relatively small size of the training set and the highly diverse sequences it contains, we would expect the pretrained models to outperform CNNs / GPs trained on one-hot encoded input to win by large margins – and in fact they do. Across other datasets, by contrast, the results are much more unclear. The protein language models sometimes achieve better performance and in other cases lose by significant margins. These results suggest some inherent limitations to the capabilities of these specific protein language models beyond the scope of this paper.

It is worth noting that an embedding derived from a protein language model can just as easily be fed into a GP as into a deep learning model, so that in the event an information-rich embedding is useful, it should benefit both GPs and deep learning models. Clearly however the choice of protein language model and embedding is challenging, since on the benchmarks we utilize here, there is no clear or consistent winner. Again, identification of an optimal representation for sequence data is beyond the scope of this paper, but is clearly a matter of substantial importance for obtaining good performance regardless of whether deep learning or a GP is used for modeling.

S12. Details for QM9 molecular modeling

The full QM9 dataset consists of approximately 133,000 molecules. To be consistent with other authors, we first remove those molecules for which Ramakrishnan et al. indicate that the geometry-optimized structure failed consistency checks. We then split the remaining data randomly into a training set of 110,000, a validation set of 10,000, and a test set of 10,831 using random seed 123.

For the SOAP descriptors as implemented in the dscribe library, there are several hyperparameters we can tune:

- 1) The standard deviation of the Gaussians used to represent the atoms in the neighborhood of the central atom (sigma);
- 2) Rcut, or the radius at which an atom is considered "outside the neighborhood" and no longer included in the representation;
- 3) Weighting, i.e. reduced weighting for atoms further from the central atom (several different schemes provided).

There are also the number of radial basis functions, *n_max*, and the number of spherical harmonics, *l_max*. These improve the accuracy of the representation if increased, but also dramatically increase the size of the descriptor vector. We settled on 12 for n_max and 9 for l_max, the same values used by Willatt et al.³², since we did not want to use a larger descriptor vector size for this study. Even this configuration however generates roughly 18,000 features per atom.

We started from the weighting scheme and weights identified as optimal by Willatt et al.³², who used power weighting in which an atom within the distance *rcut* is weighted based on its distance using the expression:

$$\frac{1}{1+\left(\frac{r}{r_0}\right)^m}$$

For all of the SOAP feature hyperparameters we used the values selected by Willatt et al. based on their grid search with two exceptions: we optimized *rcut*, or the cutoff distance, and *r0* from the weighting scheme shown above, using the values from Willatt et al. as a starting point. We tuned *r0* and *rcut* by evaluating the marginal likelihood on a randomly selected subset of the training data consisting of 25,000 datapoints. In initial experiments, we found that we could achieve almost the same accuracy by generating features for heavy atoms (i.e. non-hydrogen) only and omitting the hydrogens. After tuning, we adopted the following settings for dscribe:

N_max: 12

L_max: 9 Sigma: 0.25 R_cut: 3.25

Weighting: Power

R0: 1.5 M: 9

M and *r0* determine how rapidly the weighting falls off from the central atom. We generate SOAP features for each atom individually; since each molecule in this dataset has up to 9 heavy atoms, each molecule has up to 9 descriptor vectors corresponding to these atoms. These can be used as inputs to either the graph convolution kernel or graph polynomial kernel described in the main text. We divide the SOAP descriptors for each atom by the norm of the descriptor vector so that each descriptor vector is unit-norm; this ensures that if the GraphPoly kernel is used, it will have the same interpretation as the original SOAP kernel.

To tune the kernel hyperparameters, we use the standard workflow from Figure 2c of the main text. We begin by finding a starting point using matrix decomposition based marginal likelihood, then optimize with a larger number of random features (16,384) using Bayesian optimization. This procedure took 4 hours on a single A6000 GPU. All hyperparameter tuning was performed using internal energy at 298K as a target. The same hyperparameters that work well for internal energy at 298K also work well for the other objectives as illustrated. We then fit the final model using either 16,384 random features, 32,768 random features or 66,536 random features. The results appear in Table 4 of the main text.

As expected, we can "buy" small improvements in performance by using a larger number of random features, but even 16,384 random features is sufficient to achieve a mean absolute error 5x smaller than chemical accuracy. Consequently, in practice using larger numbers of random features has limited usefulness and it would be perfectly fine to use 16,384 random features for this problem. Moreover, the most important target for further improvement is likely the SOAP features themselves. The large number of SOAP features generated per atom greatly increases computational expense, since many features must be generated, saved and loaded from disk while processing each minibatch of data when iterating across the dataset. Furthermore, it constrains our ability to improve the accuracy of the model by increasing the number of basis functions. Multiple authors have suggested more compact representations that achieve similar or better accuracy. A more compact representation would enable us to increase the number of basis functions, thereby improving the accuracy of the model, while decreasing the length of the feature vector, thereby reducing its computational expense. We regard this as an important area for further work.

It is interesting to note the advantages provided by our fast Hadamard transform based Conv1d kernel (FHTConv1d) here as well. If we were to use the Conv1d kernel instead, to generate 66,536 random features with 18,000 input features, we would require a matrix with roughly 1.2 billion floats! The FHTConv1d kernel, by contrast, needs to store roughly 288,000 8-bit integers and 72,000 floats – a dramatic reduction in memory footprint.

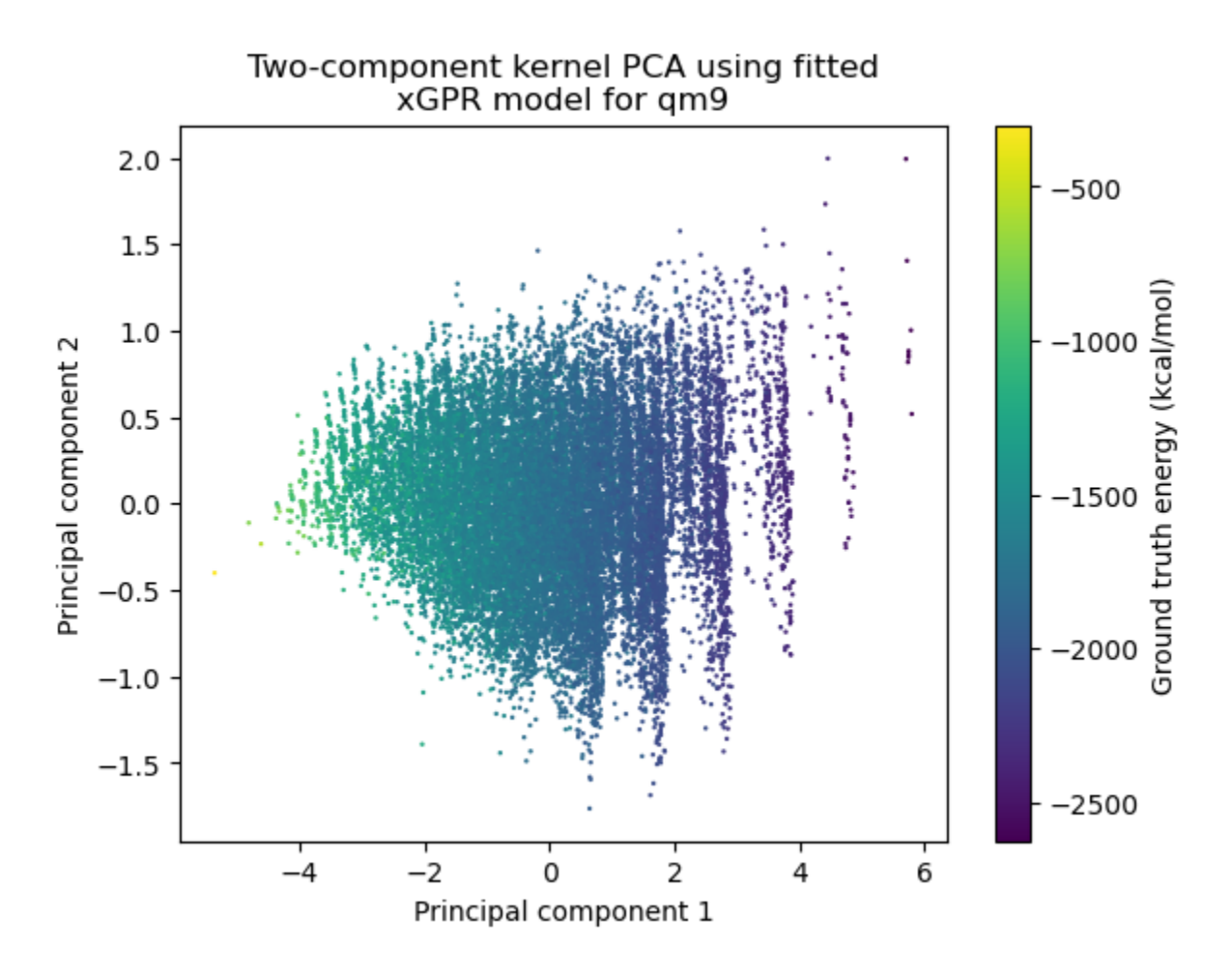
S13. Clustering and kernel PCA using representations generated by xGPR

For this example, we use the QM9 dataset. Out of the approximately 130,000 molecules in the dataset, we randomly select 20,000 as a test set. We encode each atom and its neighbors using

one-hot encoded, out to the 15th most distant neighbor (an arbitrary cutoff). Each one-hot encoded neighbor is weighted by 1 / distance**6; the 6th power used here corresponds to the weighting used in the London matrix sometimes used as a representation for machine learning on small molecules. We then follow the standard workflow by tuning hyperparameters first using a smaller number of random features (2048) with a matrix-decomposition based procedure, then "fine-tune" using a larger number of random features (8192) with an approximate marginal likelihood procedure. The code used to encode the molecules and tune the hyperparameters is provided in the small molecule tutorial in the xGPR documentation, available online at https://xgpr.readthedocs.io/en/latest/. As illustrated, depending on the number of random features employed for fitting, this model can achieve a mean absolute error < 1.1 kcal/mol.

Next, we use the kernel_xpca tool provided in the visualization_toolkit module of xGPR version 0.0.2.1 to retrieve the top 500 principal components. We use the top 2 principal components to generate the kernel PCA plot below in Figure S5, for the test set data only.

Figure S5. Kernel PCA on the QM9 test set, using the GraphConv-1d kernel



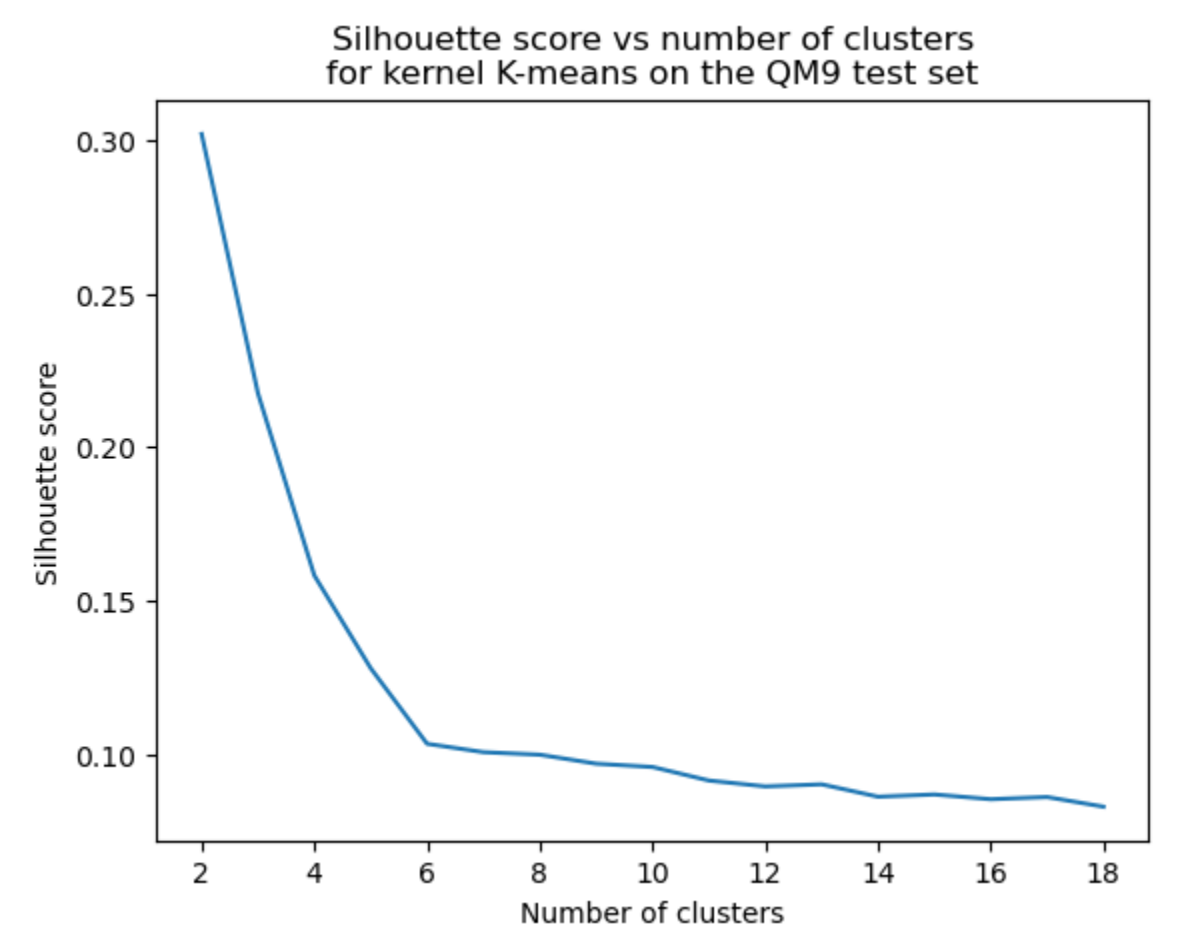
As illustrated, the top principal component correlates nicely with the ground-truth label we want to predict (energy at 298K). This will not always be the case, because a great deal of information is obviously discarded by using a 2d representation in place of the 16,384 dimensional representation generated by xGPR. To further explore the data, then, we perform k-means clustering using the scikit-learn library with the top 500 principal components as input,

using the silhouette score to assess the performance of a given number of clusters. This operation approximates performing kernel k-means clustering on the original input data using a GraphConv-1d kernel.

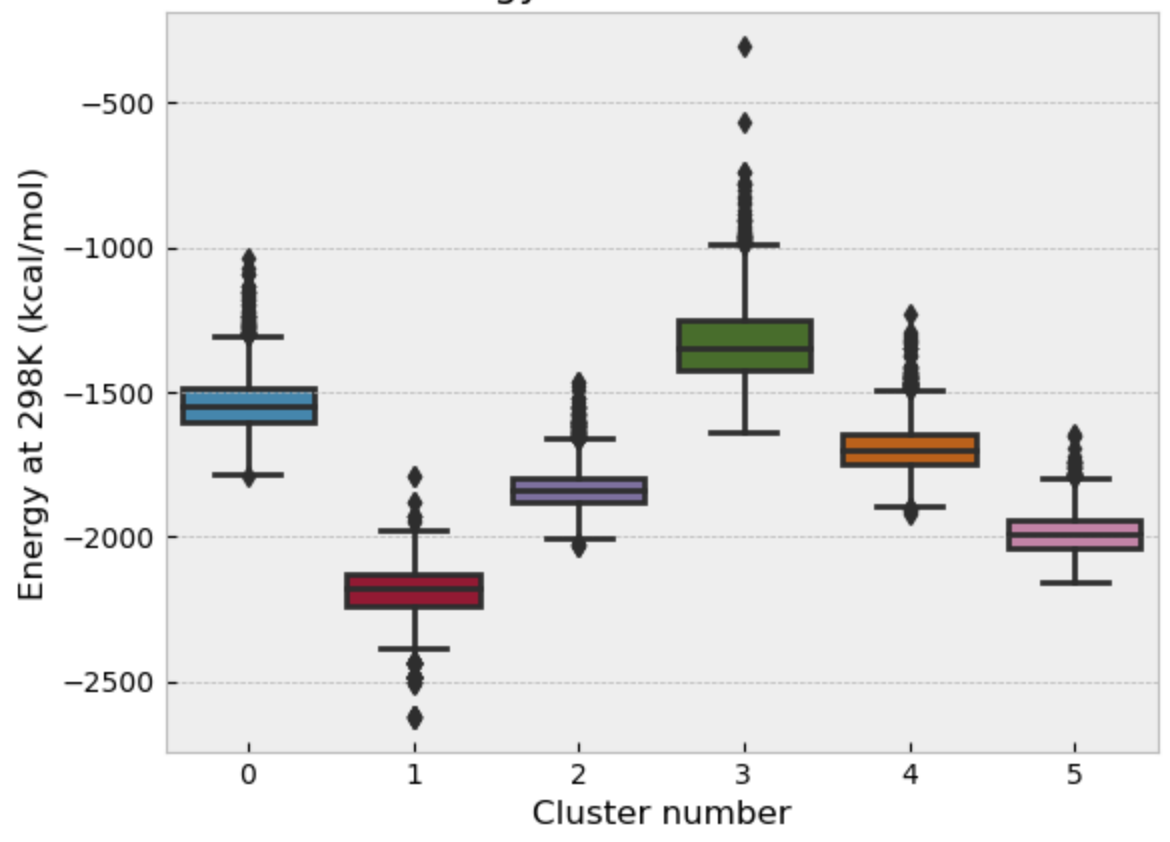
The silhouette score plot appears in Figure S6a; this result strongly suggests 6 clusters is appropriate, and thus we fit the final k-means model using 6 clusters. The distribution of energy at 298 K in each resulting cluster appears in Figure S6b, and the distribution of topological polar surface area (TPSA) in each cluster appears in Figure S6c. We see that the kernel has grouped the data in a way that reflects some interesting properties of the input data, including the one we are trying to predict. This type of exploratory analysis can help us understand both the distribution of our original data, the appropriateness of the kernel for the selected task, and the means by which the model makes predictions.

Figure S6. Kernel k-means clustering of the QM9 test set, using the GraphConv-1d kernel

Α

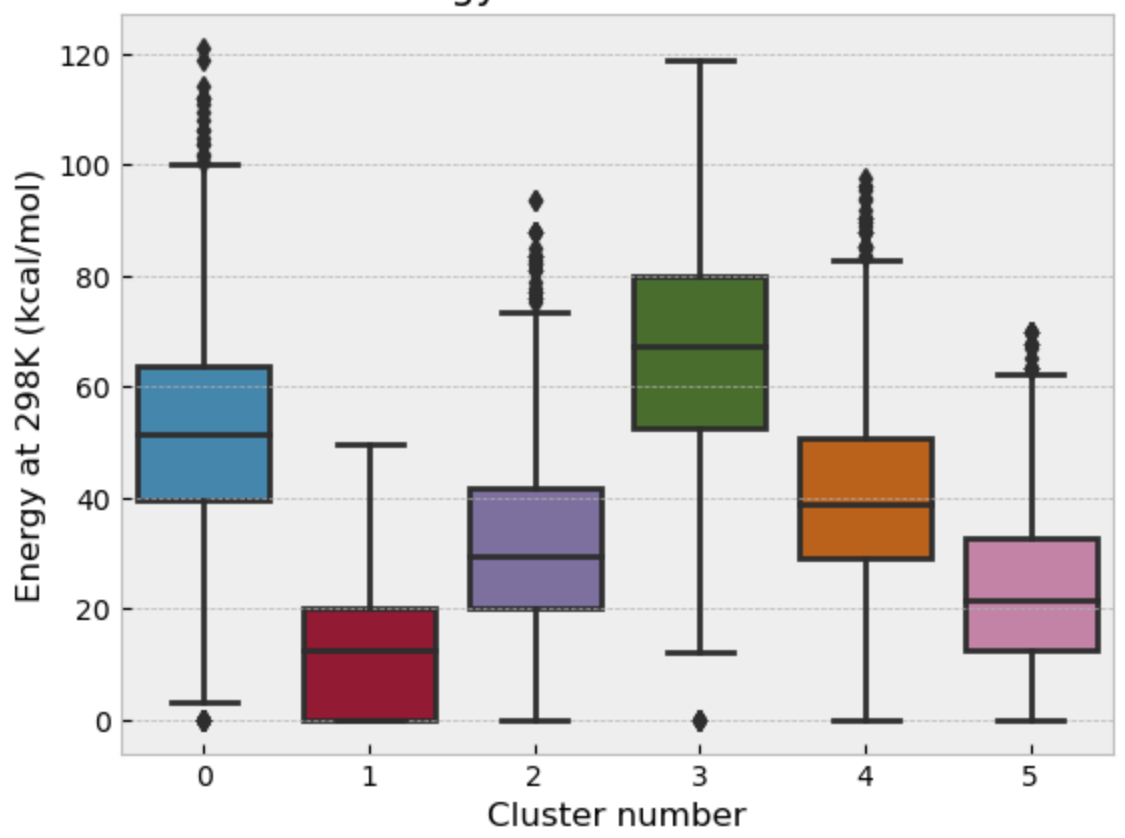


The one-hot encoded QM9 dataset clustered using the random features representation from xGPR: energy vs cluster number



С

The one-hot encoded QM9 dataset clustered using the random features representation from xGPR: energy vs cluster number



References

- Bertin-Mahieux, T., Ellis, D. P. W., Whitman, B. & Lamere, P. The Million Song Dataset.
 591–596 (2011) doi:10.7916/D8NZ8J07.
- Qian, N. & Sejnowski, T. J. Predicting the secondary structure of globular proteins using neural network models. *J. Mol. Biol.* 202, 865–884 (1988).
- 3. Corke, P. I. A robotics toolbox for MATLAB. IEEE Robot. Autom. Mag. 3, 24–32 (1996).
- Dallago, C. et al. FLIP: Benchmark tasks in fitness landscape inference for proteins. Proc. Neural Inf. Process. Syst. Track Datasets Benchmarks 1, (2021).
- 5. Rao, R. *et al.* Evaluating Protein Transfer Learning with TAPE. *ArXiv190608230 Cs Q-Bio Stat* (2019).

- 6. Ramakrishnan, R., Dral, P. O., Rupp, M. & von Lilienfeld, O. A. Quantum chemistry structures and properties of 134 kilo molecules. *Sci. Data* **1**, 140022 (2014).
- 7. Hensman, J., Fusi, N. & Lawrence, N. D. Gaussian Processes for Big Data. (2013).
- 8. Bauer, M., van der Wilk, M. & Rasmussen, C. E. Understanding Probabilistic Sparse
 Gaussian Process Approximations. in *Advances in Neural Information Processing Systems*vol. 29 (Curran Associates, Inc., 2016).
- 9. Reed, M. & Simon, B. *Methods of Modern Mathematical Physics. I: Functional Analysis*. vol. II (Academic Press, 1975).
- 10. Sutherland, D. J. & Schneider, J. *On the Error of Random Fourier Features*. http://arxiv.org/abs/1506.02785 (2015) doi:10.48550/arXiv.1506.02785.
- 11. Rasmussen, C. & Williams, C. Gaussian Processes for Machine Learning. Vol. 2. No. 3. Cambridge, MA: MIT press, 2006. vol. 2 (MIT Press, 2006).
- Choromanski, K. et al. The Geometry of Random Features. in Proceedings of the
 Twenty-First International Conference on Artificial Intelligence and Statistics 1–9 (PMLR, 2018).
- 13. Cho, Y. & Saul, L. Kernel Methods for Deep Learning. in *Advances in Neural Information Processing Systems* vol. 22 (Curran Associates, Inc., 2009).
- Yu, F. X. X., Suresh, A. T., Choromanski, K. M., Holtmann-Rice, D. N. & Kumar, S.
 Orthogonal Random Features. in *Advances in Neural Information Processing Systems* vol.
 (Curran Associates, Inc., 2016).
- 6. Krylov Subspace Methods, Part I. in *Iterative Methods for Sparse Linear Systems* 151–216 (Society for Industrial and Applied Mathematics, 2003).
 doi:10.1137/1.9780898718003.ch6.
- 16. 10. Preconditioning Techniques. in *Iterative Methods for Sparse Linear Systems* 283–351
 (Society for Industrial and Applied Mathematics, 2003). doi:10.1137/1.9780898718003.ch10.
- 17. Williams, C. & Seeger, M. Using the Nyström Method to Speed Up Kernel Machines. in

- Advances in Neural Information Processing Systems vol. 13 (MIT Press, 2000).
- 18. Kumar, S., Mohri, M. & Talwalkar, A. Sampling Methods for the Nystro m Method. 26.
- Alaoui, A. & Mahoney, M. W. Fast Randomized Kernel Ridge Regression with Statistical Guarantees. in *Advances in Neural Information Processing Systems* vol. 28 (Curran Associates, Inc., 2015).
- 20. Martinsson, P.-G. & Tropp, J. Randomized Numerical Linear Algebra: Foundations & Algorithms. Preprint at http://arxiv.org/abs/2002.01387 (2021).
- 21. Li, H. *et al.* Algorithm 971: An Implementation of a Randomized Algorithm for Principal Component Analysis. *ACM Trans. Math. Softw. Assoc. Comput. Mach.* **43**, 28 (2017).
- Halko, N., Martinsson, P.-G. & Tropp, J. A. Finding structure with randomness: Probabilistic algorithms for constructing approximate matrix decompositions. Preprint at http://arxiv.org/abs/0909.4061 (2010).
- 23. Boutsidis, C. & Gittens, A. Improved matrix algorithms via the Subsampled Randomized Hadamard Transform. Preprint at http://arxiv.org/abs/1204.0062 (2013).
- 24. Frangella, Z., Tropp, J. A. & Udell, M. Randomized Nystr\"om Preconditioning. Preprint at http://arxiv.org/abs/2110.02820 (2021).
- 25. Ubaru, S., Chen, J. & Saad, Y. Fast Estimation of \$tr(f(A))\$ via Stochastic Lanczos Quadrature. *SIAM J. Matrix Anal. Appl.* **38**, 1075–1099 (2017).
- Han, I., Malioutov, D. & Shin, J. Large-scale Log-determinant Computation through Stochastic Chebyshev Expansions. http://arxiv.org/abs/1503.06394 (2015)
 doi:10.48550/arXiv.1503.06394.
- 27. Saibaba, A. K., Alexanderian, A. & Ipsen, I. C. F. Randomized matrix-free trace and log-determinant estimators. *Numer. Math.* **137**, 353–395 (2017).
- 28. Gardner, J. R., Pleiss, G., Bindel, D., Weinberger, K. Q. & Wilson, A. G. GPyTorch: Blackbox Matrix-Matrix Gaussian Process Inference with GPU Acceleration. Preprint at https://doi.org/10.48550/arXiv.1809.11165 (2021).

- 29. Hutchinson, M. F. A stochastic estimator of the trace of the influence matrix for laplacian smoothing splines. *Commun. Stat. Simul. Comput.* **19**, 433–450 (1990).
- 30. Bartók, A. P., Kondor, R. & Csányi, G. On representing chemical environments. *Phys. Rev. B* **87**, 184115 (2013).
- 31. Wacker, J., Ohana, R. & Filippone, M. Complex-to-Real Random Features for Polynomial Kernels. Preprint at https://doi.org/10.48550/arXiv.2202.02031 (2022).
- 32. Willatt, M. J., Musil, F. & Ceriotti, M. Feature Optimization for Atomistic Machine Learning Yields A Data-Driven Construction of the Periodic Table of the Elements. *Phys. Chem. Chem. Phys.* **20**, 29661–29668 (2018).